https://doi.org/10.5194/egusphere-2025-2577
Preprint. Discussion started: 3 July 2025

Dynamics of inorganic nitrogen cycling, redox conditions, and microbial community composition in a floodplain soil induced by a heavy rainfall after summer drought

Johanna Schlögl[1], Clemens Karwautz[2], Lena Cramaro[2], Wolfgang Wanek[3], Judith Prommer[3], Theresa Böckle[3], Andreas Kappler[4], Stefan B. Haderlein[1], Christian Griebler[2]

[1]Environmental Mineralogy, Department of Geosciences, University of Tübingen, Schnarrenbergstraße 94-96, 72076 Tübingen, Germany

[2]Department of Functional and Evolutionary Ecology, Division of Limnology, University of Vienna, Djerassiplatz 1, 1030 Vienna, Austria

[3]Division of Terrestrial Ecosystem Research, Department of Microbiology and Ecosystem Science, Center of Microbiology and Environmental Systems Science, University of Vienna, Djerassiplatz 1, 1030 Vienna, Austria

[4]Geomicrobiology, Department of Geosciences, University of Tübingen, Schnarrenbergstraße 94-96, 72076 Tübingen, Germany

Correspondence to: Christian Griebler (christian.griebler@univie.ac.at), Stefan B. Haderlein (stefan.haderlein@uni-tuebingen.de)

Abstract. Climate change increases the frequency of droughts and heavy rainfall events in temperate climates of Central Europe. This study examined the impacts of such extreme weather events on the downward transport of water and inorganic nitrogen species, the main processes governing inorganic nitrogen turnover and the dynamics of the soil microbial community in loamy floodplain soils. To this end, we conducted a field experiment simulating a heavy rainfall event applying isotopically (^{2}H) enriched water on a plot of arable land with fine-textured soil after a prolonged dry period. Subsequently the experimental plots were irrigated with non-labelled water. 50 cm deep soil cores were collected from irrigated and dry control plots at different time points (days 0, 6/8 and 14) and analysed for soil nitrate and ammonium content, soil water content, ^{2}H-enrichment of soil water, microbial community composition based on DNA and RNA, as well as extracellular enzyme activities. Furthermore, redox potentials were recorded in situ along the soil profile on dry and irrigated plots. Whereas the irrigation water of the simulated heavy rainfall event penetrated at least 50 cm deep into the soil along preferential flow paths after only two hours, ammonium and nitrate values remained constant at 50 cm depth despite a significant decrease of nitrate in the topsoil after irrigation. This suggests that some nitrate might have been transported rapidly below 50 cm depth in contrast to ammonium, which is rather immobile in soils due to strong sorption to clay minerals. Ammonium behaved very conservatively and only increased significantly in the topsoil (0–5 cm) in response to the wetting of the dry soil ("Birch effect"). At day 6 and day 14 of the experiment, the non-labelled irrigation water of the daily recurrent moderate irrigation doses resided in the topsoil layer (0–5 cm depth) and only a small fraction penetrated to the subsoil, because the shrinkage cracks present at

https://doi.org/10.5194/egusphere-2025-2577
Preprint. Discussion started: 3 July 2025

the beginning of the experiment had closed. In parallel, the in situ redox potential dropped from > +400 mV to below -100 mV relative to the standard hydrogen electrode. Soil nitrate contents decreased when redox potentials were below +100 mV and vice versa. This implies that nitrate formation and transformation after the initial rewetting was governed by soil redox conditions instead of processes induced by the rewetting after drought. Microbial community composition analysis showed no significant differences between the active fraction of the community (RNA) on irrigated and dry plots. Diversity indices on the RNA-level were somewhat higher on dry than on wet plots, although not significantly, which suggests that drying and the following rewetting selected for more adapted taxa. In contrast, activities of the extracellular enzymes β-glucosidase and exochitinase showed significantly higher activities on wet plots than on dry plots, whereas the activity of acid phosphatase did not respond to the irrigation treatment. All enzymes decreased in activity with soil depth. Overall, the heavy rainfall event had only a minor effect on the turnover of inorganic nitrogen species. Nitrogen turnover was mainly governed by redox conditions. The presence of pronounced shrinkage cracks formed after a drought period before the heavy rainfall event, however, allows for rapid nitrate dissipation into the subsoil and eventually to the underlying aquifer. Our study also showed that the soil microbial community in temperate climates reacts in terms of activity and may ultimately be reshaped to represent more resilient taxa regarding drying and rewetting cycles.

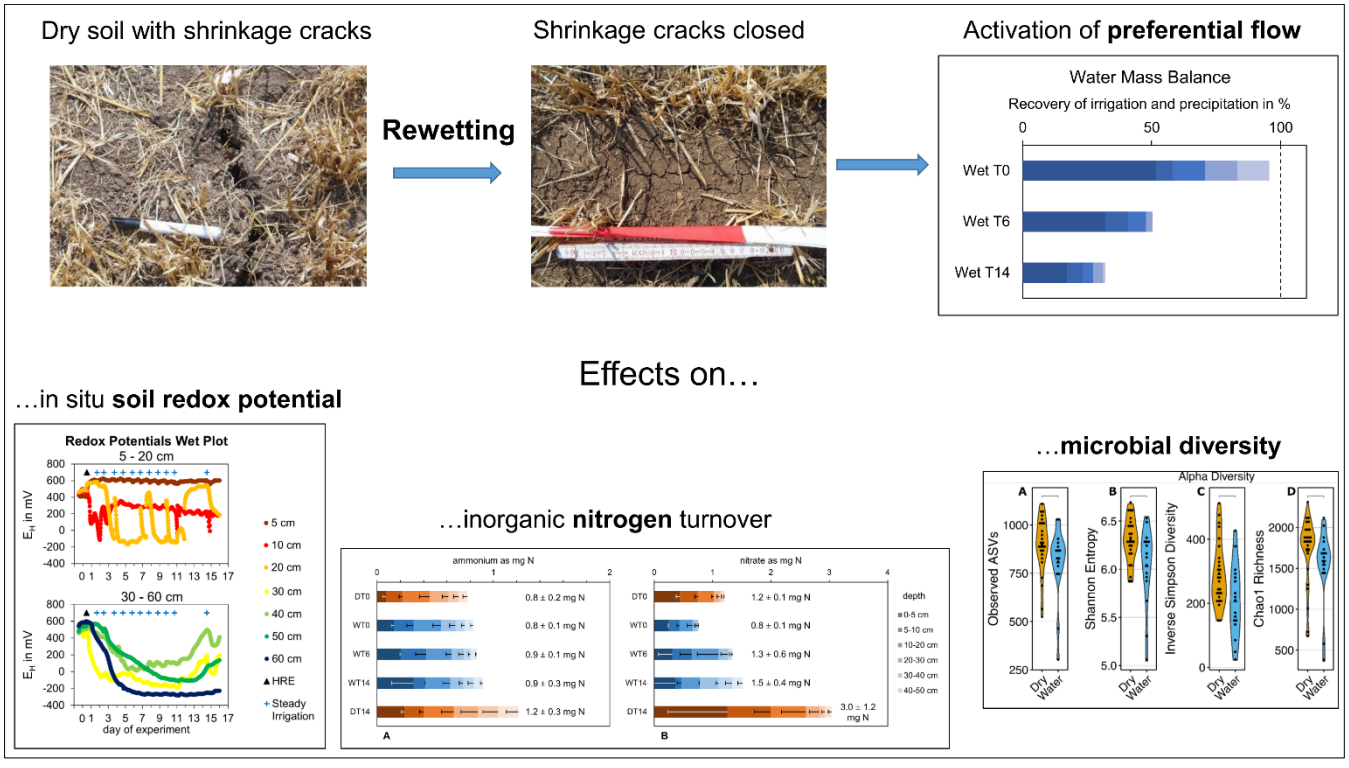

https://doi.org/10.5194/egusphere-2025-2577
Preprint. Discussion started: 3 July 2025

1 Introduction

Floodplains are important landscape compartments when it comes to nitrogen turnover (Lair et al., 2009; Venterink et al., 2003). Often, floodplain soils are exposed to recurrent inundation and dry periods, or they are influenced by alternating groundwater levels throughout the year (Baldwin and Mitchell, 2000; Coby et al., 2011). In both cases, they experience alternating oxygen availability and thus fluctuating redox conditions. The availability of oxygen determines which nitrogen turnover processes dominate (Baldwin and Mitchell, 2000; Hefting et al., 2004). Inorganic nitrogen in the form of ammonium is released during the mineralization of organic matter. Ammonium is relatively stable under reducing conditions but is nitrified under oxidizing conditions. Under reducing conditions, nitrate is mainly denitrified to N_2O and N_2 via nitrite and NO.

Climate change increases the frequency and amplitude of weather extremes such as drought periods and heavy rainfall events (Coumou and Rahmstorf, 2012; Horton et al., 2016; Perkins et al., 2012). Heavy rainfall after summer drought triggers important hydrological and biogeochemical processes, particularly in fine-textured, loamy soils. First of all, drought causes the formation of shrinkage cracks of substantial width and depth, that allow for preferential flow (Beven and Germann, 2013; Jarvis et al., 2016; Nimmo, 2021) and thereby fast vertical solute and particle-bound transport of nutrients and agrochemicals (Bronswijk et al., 1995; Kelly and Pomes, 1998; Schlögl et al., 2022) during a following heavy rainfall event. The two inorganic nitrogen species ammonium and nitrate differ strongly in their chemistry and biogeochemical behaviour in soils. Ammonium as a cation is prone to sorption to the mostly negatively charged soil mineral particles whereas nitrate as an anion is little sorbed in soils and therefore more mobile in pore water (Blume et al., 2016) and can thus be lost from the soil system by leaching. The fate of ammonium and nitrate during rewetting of dry soils is also determined by the so-called Birch effect. This effect describes the occurrence of a temporary flush of inorganic nitrogen after the rewetting of dry soil, that was observed in both lab (Birch, 1958, 1960) and field experiments (Cui and Caldwell, 1997). This flush of inorganic nitrogen is caused by microbial lysis, mineralization of dead microbial biomass, and by decomposition of osmoregulatory substances released by microorganisms upon rewetting (Fierer and Schimel, 2002; Jarvis et al., 2007; Saetre and Stark, 2005; Unger et al., 2010). The effect can last up to several days in the field with the main fraction of nitrogen mineralized in the first three days after wetting (Cui and Caldwell, 1997). Despite the potential importance of the Birch effect on inorganic soil nitrogen cycling, it is only triggered by severe drying-rewetting cycles. After this pulse of nitrogen seizes it is later expected that the “usual” redox-driven processes dominate soil inorganic nitrogen cycling, including mineralization, nitrification and denitrification.

Inorganic nitrogen turnover processes are largely microbiologically driven in soils. The soil microbial community adapts to regular drying and rewetting cycles (Armstrong et al., 2016; Fierer et al., 2003; Veach and Zeglin, 2020). Dependent on the frequency and intensity of the disturbance in hydraulic and redox conditions, dynamics of microbial community composition and activities may respond differently (Moche et al., 2015; Rinklebe et al., 2006). In mid-European temperate climates such as at our study site, drying and rewetting cycles might become more frequent in the future due to climate change (Coumou and Rahmstorf, 2012; Horton et al., 2016; Perkins et al., 2012). It is therefore important to understand their effects on microbial community activity and composition and related changes in soil nitrogen cycling.

https://doi.org/10.5194/egusphere-2025-2577
Preprint. Discussion started: 3 July 2025

The objectives of our study were (i) to evaluate the water flow and solute transport during a drying-rewetting event induced by heavy rainfall following a summer drought in a fine-textured floodplain soil, (ii) to examine the temporal transition from pulse-driven nitrogen cycling (the Birch effect) upon soil rewetting towards redox-driven nitrogen turnover processes, and (iii) to assess the impact of drying and rewetting on soil microbial community structure and activity. To this end, we conducted a field experiment simulating a one-hour heavy rain event followed by recurrent moderate daily rainfall for 14 days on a Gleysol that exhibited pronounced shrinkage cracks after summer drought. The water of the heavy rainfall event was spiked with deuterated water as a conservative hydrological tracer, that allowed us to quantify water infiltration depth and distribution. We monitored depth-resolved in situ redox potentials using permanently installed sensors and took soil cores to 50 cm depth from irrigated and dry control plots on day 0, i.e., two hours after the heavy rainfall simulation, on day 6/8 and on day 14. The soil samples were analyzed for vertical changes in soil water content, in isotopic signatures (δ^2H) of the pore water, in extractable ammonium and nitrate concentrations, in total (DNA-level) and active (RNA-level) microbial community composition, as well as in extracellular enzyme activities.

2 Materials and Methods

2.1 Study site

The study site is located in the Ammer valley floodplain, approx. 7 km West of Tübingen in SW Germany (48.521266° N, 8.972687° E, 394 m a.s.l.). The catchment of river Ammer is situated in the South German Escarpment in the geological units of the Middle and Upper Triassic. The west of the catchment lies within the Muschelkalk unit whereas the eastern part lies within Keuper units, which mostly consist of terrestrial sediments, such as sand-, mud- or dolostones (Geyer et al., 2011; Grathwohl et al., 2013; Martin et al., 2020; Schwientek et al., 2013).

The floodplain with the study site lies in the eastern part of the catchment and is defined by Keuper hills at its southern and northern rim. The hydrostratigraphy within the floodplain comprises from bottom to top: Keuper rocks as basement, an aquifer mainly made of gravel and clay (gravel aquifer), a regional aquitard (lower clay aquitard), a confined aquifer made of calciferous tufa sediments (tufa aquifer) and another regional aquitard (upper clay aquitard) (Martin et al., 2020). The upper clay aquitard comprises the investigated soil. On average, it is 2 m thick and consists of fine-grained, clay mineral-rich alluvial sediments from the surrounding Keuper hills. The bottom half of this aquifer is water saturated throughout the year. The soils are characterized as Gleysols, showing the typical gleyic properties such as color-distinguishable reduced and oxidized horizons (Appendix A) (Martin et al., 2020). In the present study the cores of 50 cm depth only sampled the Ah and the Go horizon.

The soil has an organic matter content (quantified as total organic carbon (TOC), for methodological details see Appendix B) of 2–2.5 wt% in the upper 15 cm and of 1 wt% at 15 to 50 cm depth (Appendix B). It has a uniform soil texture of 11 ± 4 wt% of sand, 56 ± 6 wt% of silt and 32 ± 4 wt% of clay within the upper 50 cm (Appendix C, determined after DIN EN ISO 17892-

https://doi.org/10.5194/egusphere-2025-2577
Preprint. Discussion started: 3 July 2025

4). The soil pH varied between 7.0 and 7.3 and was determined on six samples from irrigated plots, two each from soil depths of 0–10 cm, 20–30 cm and 40–50 cm, after stirring the sample in a 1 : 1 (v : w) mix with deionized water for 30 min.
The experiment was conducted on a plot of arable land after summer barley harvest and after a prolonged dry period during summer (see Section Meteorological Conditions for more details below). Information about the previous use of the plot was provided by personal communication with the farmer: During winter 2018/19 before cropping of summer barley a catch crop (radish and mustard) was planted and in February 2019 this green manure was incorporated into the soil with a cultivator. The plot was fertilized with horse manure in winter 2018/19 and with calcium ammonium nitrate fertilizer (27 % N) in spring 2019. During cultivation of summer barley, the herbicide Ariane-C (active ingredients: 100 g L^{-1} Fluroxypyr (as Methylheptylester 144 g L^{-1}), 80 g L^{-1} Clopyralid + 2.5 g L^{-1} Florasulam) was applied.

2.2 Meteorological conditions

The climate in the region of the experimental site is temperate oceanic with a long-term mean annual precipitation of 718 mm and a mean annual temperature of 9.4°C (1981–2010, (German meteorological service (Dwd), 2024)). From a weather station in Tübingen Unterjesingen (48.52950° N, 8.98380° E, 439 m a.s.l., close to the actual experimental site) meteorological data were retrieved (Agrarmeteorologie baden-Württemberg, 2021) (Appendix D). The experiment was conducted from 16 to 30 July 2019. In the two weeks preceding experimental start, temperatures well above 20°C dominated on all but two days and three moderate (according to the classification of the American meteorological society (2012)) rainfall events occurred (9.1, 5.1, and 33.1 mm, respectively). During the experiment, a minimum temperature of 10.2°C was reached during night (night average 17.7°C) and a maximum temperature of 36.3°C during daytime (day average 24.5°C). On 12 days, temperatures > 25°C and on six of these temperatures > 30°C were measured. Following the FAO guideline (Allen et al., 1998), the reference evapotranspiration ETo for July 2019 was calculated as 4.2 mm day^{-1} (see Appendix E for details on the calculation). From 16 to 30 July 2019, two natural rainfall events occurred, one on the 21 July from 02:00 to 05:00 am (2.5 mm) and a heavy rainfall event from 26 July 08:00 pm to 27 July 05:00 am (24.7 mm) (Appendix D). During both of these events, the dry control plots were covered by plastic foils.

2.3 Experimental setup

2.3.1 Plot design

The plot design comprised nine plots that were arranged as a Latin Square with three different treatments (Figure 1). All plots were of 2.4 m lateral length and separated by 50 cm stripes to allow access. Within each plot a sampling area of 2 m x 2 m was defined to exclude boundary effects. Three different treatments were realized, but only two are relevant for the study presented here: (i) W plots were artificially irrigated to simulate a heavy rainfall event (HRE) after a dry period, (ii) D plots

https://doi.org/10.5194/egusphere-2025-2577
Preprint. Discussion started: 3 July 2025

remained dry and served as controls. The third treatment included the application of glyphosate before irrigation. Results from these plots are presented in other publications (Schlögl et al., 2022; Wirsching et al., 2022).

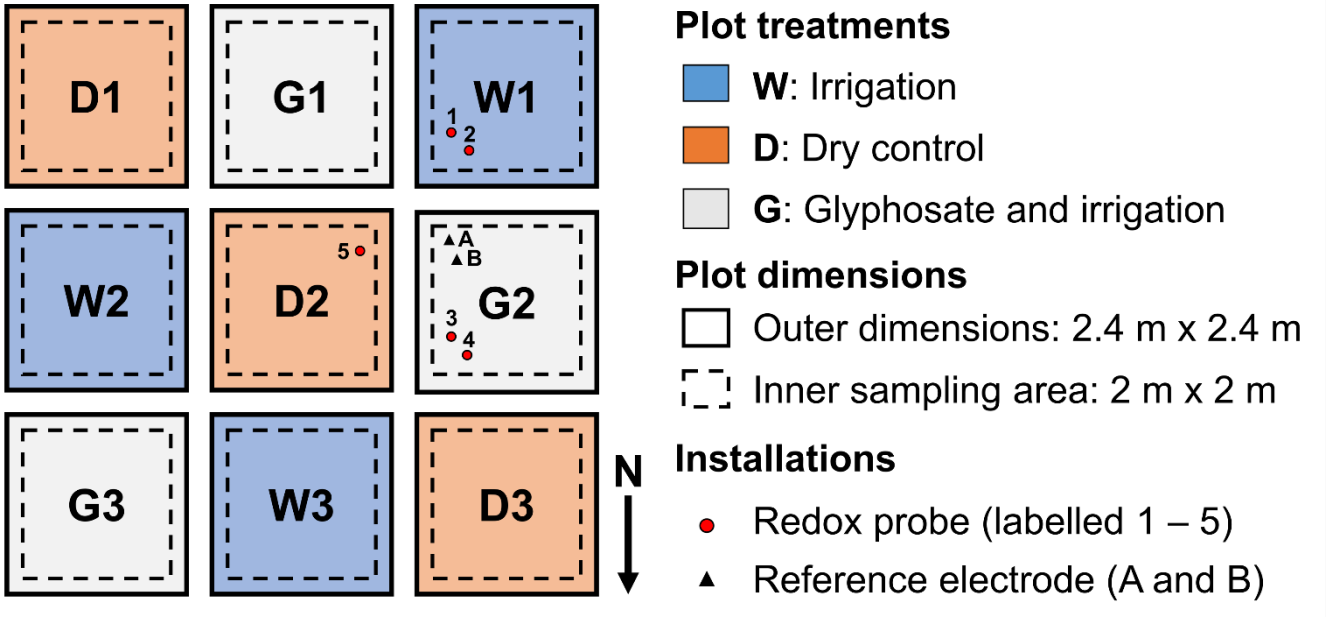

Figure 1: Plot design and treatments in the field experiment. Nine plots of 2.4 m x 2.4 m lateral length were arranged as a Latin Square and three treatments were realized in triplicates: A heavy rainfall event was simulated at day 0 and light daily irrigation followed for 14 days (W plots, blue). D plots (orange) remained dry and served as control plots. G plots (grey) were treated with glyphosate before they received the same rainfall treatment as W plots. An inner sampling area (dashed line) was defined to minimize boundary effects. For the in situ monitoring of redox potentials, redox sensors (red circles) were installed on plots W1, D2 and G2, and two reference electrodes (black triangles A and B, where B served as control for the system) were installed on plot G2 approx. in equidistance to all redox sensors. (Figure adapted after Schlögl et al. (2022).)

2.3.2 Plot treatment

Irrigation took place from the 16 to 31 July 2019 with the day of the simulated heavy rainfall event (16 July) defined as day 0 (T0) (Figure 2). All plots were covered for one week before the experiment to guarantee dry initial conditions. The heavy rainfall event (defined as 7.6 to 50 mm per hour by the American meteorological society (2012)) was simulated by irrigation with 24.3 mm deionized water for approx. one hour with watering cans. The water was labelled with deuterated water (D_2O) as a conservative tracer. Two liters of deuterated water (99.9 atom %, Carl Roth, Germany) were mixed with the irrigation water (1000 L) which resulted in an input δ^2H signature of 12 730 ‰ vs. Vienna Standard Mean Ocean Water (VSMOW). On days 1 to 10 and on day 14, light irrigation with non-D_2O-labeled water was conducted with an irrigation rate of 5.2 mm day^{1}

https://doi.org/10.5194/egusphere-2025-2577
Preprint. Discussion started: 3 July 2025

to keep the soils moist and to force closure of shrinkage cracks to investigate the development and influence of in situ redox potential on nitrogen turnover processes and on the microbial community.

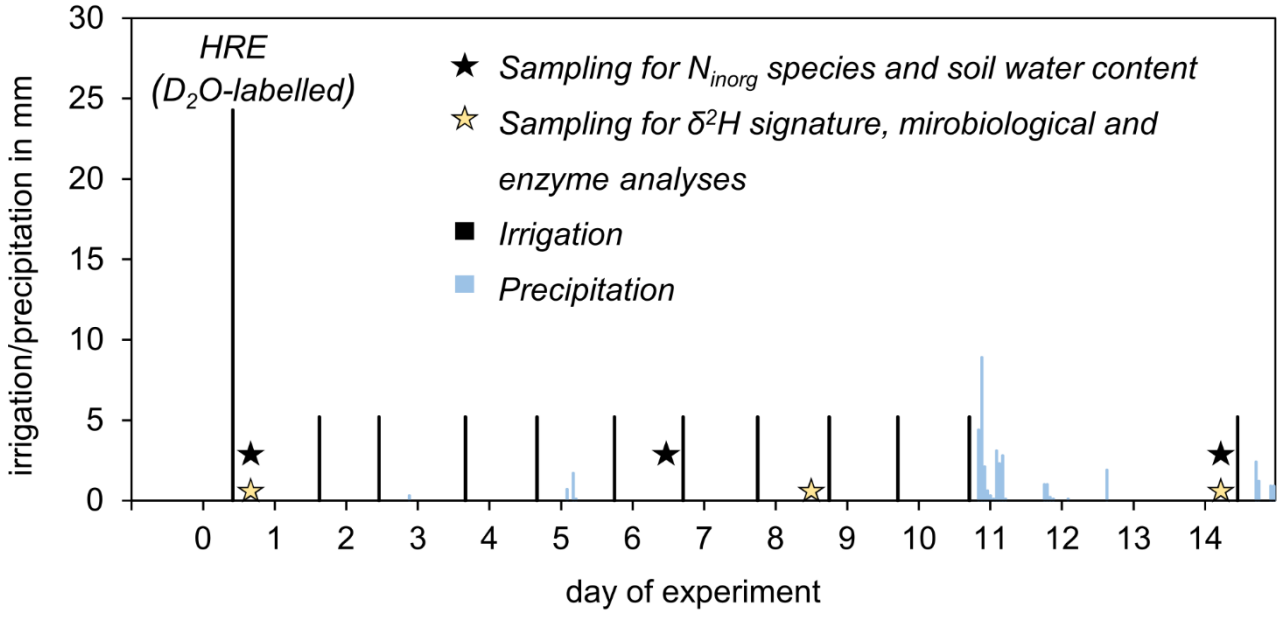

Figure 2: Irrigation and sampling scheme. Irrigation (black bars, length indicates intensity) included a simulated heavy rainfall event (HRE) with D_2O-labeled water on day 0 followed by light daily irrigation on W plots. Natural precipitation is indicated by light blue bars, which was excluded from D plots but not from W plots. Sampling for inorganic nitrogen species (N_{inorg}) and soil water content took place on days 0, 6 and 14 (black stars), samples for analyses of δ^2H signature, microbial communities and enzymes were retrieved on days 0, 8 and 14 (golden stars). (Figure adapted after Schlögl et al. (2022).)

2.3.3 Sampling

Sampling was done with a stainless-steel soil corer (Humax, Hasli-Rüegsau, Switzerland). The soil cores were retrieved within PVC liners of 50 cm length and 3.5 cm diameter and immediately put on dry ice. In the lab, they were stored at -80°C (microbiological analyses, enzyme analyses, δ^2H analyses) and at -21°C (inorganic nitrogen species) until further analysis. The holes in the field were filled with bentonite.

The sampling scheme comprised sampling for (i) inorganic nitrogen species and soil water content, and (ii) for soil pore water δ^2H, microbial community structure, and soil enzymes (Figure 2). For the analysis of soil water δ^2H, cores were taken from W plots along shrinkage cracks. Additional samples were taken from D plots to determine the natural δ^2H background. Samples for inorganic nitrogen species, soil water content and microbiological analyses were taken from W and D plots along shrinkage cracks. The initial shrinkage cracks were marked before the first irrigation so that during later stages of the experiment, their

https://doi.org/10.5194/egusphere-2025-2577
Preprint. Discussion started: 3 July 2025

course was still recognizable. Sample codes in the following text are as follows: treatment of the respective plot (dry (D), irrigated (W)) followed by the respective experimental replicate number (1, 2 or 3) as well as the time point T + number, where the number expresses the day. For example, W1T8 refers to the irrigated plot W1 sampled at day 8, while WT8 refers to all three replicate W plots on day 8.

2.3.4 In situ monitoring of redox potentials

To evaluate the redox potential as a controlling factor of the microbial turnover of the two inorganic nitrogen species, nitrate and ammonium, in situ soil redox potentials were measured on a plot irrigated with water (plot W1) with two independent redox sensors (sensor 1 and 2) and on a dry control plot (plot D2) with one sensor (sensor 5) (Figure 1). The multilevel redox sensors (PaleoTerra, Oijen, The Netherlands) were made of fiberglass and epoxy tubes and were of 1.20 m length. Each sensor had 10 platinum (Pt) electrodes. For the installation of the sensors, we first drilled a vertical hole into the soil that was 2 mm smaller in diameter than the sensors, so that after sensor installation, the contact between the electrodes and the soil was given. Then the sensors were installed in a way that the first electrode was placed 5 cm below ground level (bgl) and the further electrodes at 10 cm intervals bgl. Two Ag/AgCl reference electrodes (A and B) (KCl sat.; $E^0 = 0.199$ V) were installed on plot G2 (Figure 1). One of them served as the reference electrode for the measurements, the other one as a control for the system. Measured redox potentials (E_{meas}) are reported vs. the standard hydrogen electrode (SHE; $E^0 = 0$ V, by definition) as $E_H = E_{meas} + E_{KCl,sat}$. Measurement precision was ± 10 mV. The sensors and the reference electrodes were connected to a data logger (Campbell Scientifc, Logan, Utah, US) which stored the redox potentials at 30-minute intervals throughout the experiment. The characterization of the in situ soil redox conditions will be based on the following categorization (Mansfeldt, 2003) of E_H values at circumneutral pH: oxidizing (> +400 mV vs. SHE), weakly reducing (+400 to +200 mV), moderately reducing (+200 to -100 mV) and strongly reducing (< -100 mV).

2.3.5 Soil water content

For the assessment of gravimetric soil water content on irrigated (W) and dry (D) plots, the 50 cm cores were cut into increments of 5 cm for 0–10 cm depth and into increments of 10 cm for 10–50 cm depth. From these increments, triplicates of approx. 1.5 g of field wet soil (scale precision 0.001 g) were weighed (small pebbles were rejected) before and after freeze drying. The gravimetric water content (g g^{-1}) was calculated as the ratio of water loss to dry weight. The soil water content of the D plots on day 0 was used as reference and is hereafter referred to as “initial soil water content”.

2.4 Chemical and isotopic analyses

2.4.1 δ^2H signature of soil water

The δ^2H signature of the soil pore water was determined by H_2O(liquid)-H_2O(vapor) equilibration and cavity ring-down laser spectroscopy (Picarro L2120-i and L2130-i) (Wassenaar et al., 2008). To this end, frozen core samples (cores WT0/8/14 and

https://doi.org/10.5194/egusphere-2025-2577
Preprint. Discussion started: 3 July 2025

DT0) were sliced in 10 cm segments and aliquots of 66 to 170 g of those segments were doublebagged in 1 L Ziploc freezer bags and stored at 4°C. Before analysis, the bags were filled with laboratory dry air and the bags were stored for 3 more days to let the pore water equilibrate with the headspace water vapor. Each analysis lasted up to 30 minutes until the signal plateaued, that is, stable conditions within the expected measurement accuracy were reached (i.e., standard deviation < 1.0‰ for δ^2H of the water vapor). The average signal over the last minute of the analysis was recorded. After every third sample, an internal standard (water of known isotopic composition in a freezer bag) was measured for calibration. The isotopic signatures are reported as isotope ratios relative to the international standard (Vienna Standard Mean Ocean Water, VSMOV) in delta notation in ‰ ($\delta‰ = ((R_{sample} - R_{standard})/R_{standard})*1000$), where R is the isotope ratio $^2H/^1H$ of the sample and the standard, respectively. For the determination of δ^2H background values on cores from DT0, the upper-most segment was ignored to avoid corruption by wind drift or water vapor from irrigation. Additionally, the gravimetric water content of each analyzed segment was determined by the weight difference before and after drying at 105°C. These values were used for isotope mass balance calculations.

2.4.2 Water mass balance

A water mass balance was determined to assess how much of the total irrigation plus natural precipitation received by day 0, 6 and 14 (24.3 mm, 60.0 mm and 115.0 mm, respectively) on W plots reached the different depth segments of the profile,. It was assumed that irrigation only led to a water storage change and that hardly any leaching below 50 cm occurred. The measured gravimetric soil water contents from WT0/6/14 and DT0 were converted to volumetric water contents using known bulk densities of individual depth segments. With these volumetric water contents, the amount of water volume change was calculated and the increase of water content, i.e., water volume per m² on irrigated plots, at each day was assessed by comparison with dry plots on day 0.

2.4.3 Isotope mass balance

The irrigation water of the simulated heavy rainfall event on day 0, Irr_{HRE}, was labeled with D_2O. A two-component (i.e., isotope mass balance) mixing approach was used to calculate the fraction of Irr_{HRE} in every i-th depth segment ($f_{IW,zi}$):

$$f_{IW,z_i} = \frac{\delta^2H_{z_i} - \delta^2H_0}{\delta^2H_{IW} - \delta^2H_0}$$

where δ^2H_{zi} is the measured isotope ratio in the *i*-th depth segment, δ^2H_{IW} is the isotope ratio of the simulated heavy rainfall event on day 0 (i.e., 12 730‰) and δ^2H_0 is the background average δ^2H of the pore water before irrigation (i.e., -47.6‰). For the calculation of the amount of Irr_{HRE} in each depth segment, the volumetric water content calculated as described in the Section on the water mass balance was multiplied by the fraction of irrigation water $f_{IW,zi}$.

https://doi.org/10.5194/egusphere-2025-2577
Preprint. Discussion started: 3 July 2025

2.4.4 Extraction and analysis of inorganic nitrogen

Changes in the content of inorganic nitrogen compounds nitrate and ammonium allow to follow redox transformations induced by the heavy rainfall event. Inorganic nitrogen was extracted from approx. 1.2 g of frozen soil aliquots with 12 mL 2 M KCl (p.a., Honeywell, Germany) prepared in ultrapure water (GenPure Pro UV-TOC, Thermo Fisher Scientific, Germany). Samples were shaken for 30 minutes on a horizontal shaker (IKA, Germany) with 160 motions per minute (mpm) and then centrifuged at room temperature for 15 min at 5 000 x *g* (centrifuge 5430 R, Eppendorf, Germany) and filtered (0.2 µm, regenerated cellulose, Sartorius, Germany). The extracts were stored at 4°C until analysis and were analyzed within a maximum of 2 days. Ammonium and nitrate were analyzed in these extracts by continuous flow analysis (CFA) using an AA3 HR AutoAnalyzer System from Seal Analytical (Germany). All chemicals used were purchased from Sigma Aldrich, Germany, and were of ACS grade. Standard curve range was from 0 to 7.5 mg N L^{-1} for both analytes, giving a high linearity (R^2 between 0.999 and 1.000). Nitrate determination followed the ISO 13395 standard methodology where nitrate is reduced to nitrite by hydrazine, which then reacts with sulfanilamide and NEDD forming a pink complex, which is measured at 550 nm. Potentially present nitrite in the original sample is determined independently without hydrazine addition and subtracted from nitrate concentration. Ammonium was determined according to the ISO 11732 standard methodology where it reacts with salicylate and dichloroisocyanuric acid to form a blue complex which is measured at 660 nm. To account for signal shifts due to the sample matrix (2 M KCl), standards were also prepared in 2 M KCl for both nitrogen forms.

2.4.5 Nitrate and ammonium mass balance

The measured nitrate and ammonium concentrations (mg N L^{-1}) were corrected for baseline and blank values, and the mass of nitrate and ammonium in the extraction solution was calculated. The original weight of the frozen sample was corrected to dry weight by the gravimetric water content and the mass of ammonium-N and nitrate-N per gram of dry soil was calculated. Including bulk density of the soil and the sample volume at different depths of the soil core, the mass of ammonium-N and nitrate-N at each depth interval and for the whole core was assessed.

2.5 Microbiological Analyses

2.5.1 Molecular Analysis

For molecular analysis of bacteria and archaea, soil cores were stored on dry ice immediately after sampling. Soil cores were stored in the lab at -80°C until analysis. The frozen cores were cut into segments ranging from soil depth 0–10 cm, 20–30 cm and 40–50 cm using a sterilized (2 % sodium hypochlorite solution) electric saw. For nucleic acid extraction representative subsamples (10–15 g) of the soil samples were defrosted at room temperature, homogenized with a sterile spatula, and finally duplicate aliquots of 400 mg of each subsample were used for DNA extraction.
DNA extraction was conducted with the DNeasy PowerSoil Kit (Qiagen, Hilden, Germany) according to the manufacturer's protocol. RNA was extracted using the modification of a commercial DNA extraction kit according to Tournier et al. (2015)

https://doi.org/10.5194/egusphere-2025-2577
Preprint. Discussion started: 3 July 2025

combining the FastDNA SPIN™ kit for soil (MP Biomedicals) and the RNaid® Kit (MP Biomedicals, LLC, Illkrich, France). Instead of the standard weight of 0.25 g, 0.5 g soil was used to increase the mass of RNA. RNA was purified with the RNeasy Micro Kit (Qiagen). Residual DNA was removed with DNAse I and the RNA was transcribed to cDNA using the RevertAid RT Reverse Transcription Kit (Thermo Scientific) with a random hexamer primer. A primer combination of 515F (5′-GTGYCAGCMGCCGCGGTAA-3′) and 806R (5′-GGACTACNVGGGTWTCTAAT-3′), annealing to the V4 region of the 16S rRNA was used for gene amplification, following the PCR protocol as described by Pjevac et al. (2017). Sequencing was performed on a MiSeq platform (Illumina, San Diego, CA, USA), using a v3, 600 cycle chemistry (2 × 300 b paired-end sequences) in two separate runs.

Raw reads were processed in R (version 4.1.1,) with DADA2 (v. 1.20.0) as outlined in Callahan et al. (2017). Amplicon Sequence Variants (ASVs) were inferred across all samples in pooled mode (details on sequence trimming, and quality filtering is outlined in Pjevac et al. (2017)). ASV sequences were subsequently aligned and classified using SINA version 1.7.2 and the SILVA database SSU Ref NR 99 release 138.1 using default parameters. ASVs classified as archaea, eukaryotes, mitochondria, or chloroplasts, as well as ASVs not classified at the domain level, were removed from the dataset prior to downstream analysis. Statistical data analysis was performed with R and plots were created using the package ggplot2. Alpha and beta diversity indices were calculated (vegan) and compared. Non-metric multidimensional scaling (*NMDS*) analysis of Aitchinson distances was used for ordination.

2.5.2 Extracellular Enzyme Activities

Potential activities of three soil hydrolytic enzymes, i.e., β-glucosidase (BG), N-acetylglucosaminidase (NAG; exochitinase) and acid phosphatase (AP) were measured fluorometrically with artificial substrates (Tian et al., 2023). The following 4-methylumbelliferyl (MUF) based substrates were used to measure the enzyme activities: MUF-β-D-glucopyranoside for BG, MUF-N-acetyl-β-D-glucosaminide for NAG, and MUF-phosphate for AP. Soil slurries (1:100 (w:v)) were prepared in 50 mM sodium acetate buffer (pH 5) by ultrasonication (energy input ~350 J). Substrates were added to soil slurries in black microplates in five replicates and incubated in the dark for 180 min with repeated measurements of sample fluorescence. Microplates were read by a TECAN Infinite® M200 spectrophotometer at an excitation wavelength of 365 nm and an emission wavelength of 450 nm. Sample fluorescence was corrected for quenching and the concentrations of MUF released by enzymatic activity were calibrated by respective standards added to the soil slurries.

3 Results

3.1 Soil water content and in situ redox potentials

Water mass balances and $^{2}H_2O$-isotope mass balances were calculated for days 0, 6 and 14 and days 0, 8 and 14, respectively (Figure 3a and b), to reveal flow pathways of the irrigation water. Mean values were calculated from the triplicate experimental plots for each depth section. For the water mass balance on T14 and the isotope mass balance on T8, mean values were only

https://doi.org/10.5194/egusphere-2025-2577
Preprint. Discussion started: 3 July 2025

calculated from two individual plots due to sample loss. The water mass balance (Figure 3a) included the sum of all irrigation and natural precipitation water during the experiment, Irr_{tot}, whereas the isotope mass balance (Figure 3b) only included the recovery of the D_2O-labeled heavy rainfall event (HRE) water, Irr_{HRE}.

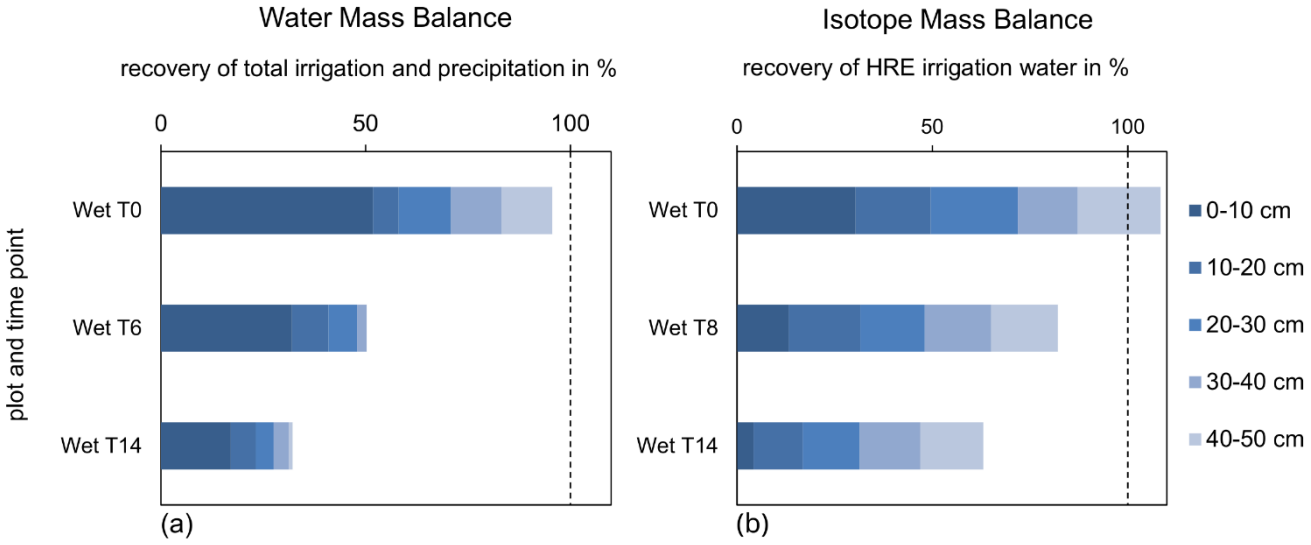

Figure 3: (a). Water mass balance for days 0, 6, and 14 (T0, 6, and 14) in five 10 cm soil depth sections. Recovery of the water is given in relation to the total amount of water that had reached the plots by irrigation and natural rainfall at the respective time point (Irr_{tot}, represented by the 100 % line). (b). Isotope mass balance for days 0, 8 and 14 (T0, T8 and T14) in five 10 cm depth intervals. Recovery of heavy rainfall water is given in relation to the amount of deuterium-labeled irrigation water of the simulated heavy rainfall event (Irr_{HRE}) on T0. The color gradient from dark to light blue indicates the depth from the top (0–10 cm) to the bottom (40–50 cm) of the soil profile.

The water mass balance was calculated as the percentage of the sum of irrigation and natural precipitation water, Irr_{tot}, recovered in the soil at days 0, 6 and 14 (T0, T6, T14) on irrigated (W) plots (Figure 3a) after subtracting pre-event water levels from dry plots. Irr_{tot} was 24.3 mm at T0, 60.0 mm at T6, and 115.0 mm at T14 which is represented as the 100 % line in Figure 3a. The recovery of irrigation plus precipitation water was 95.6 % at T0, 50.3 % at T6, and 32.1 % at T14, and thus steadily decreased during the experiment.

In the following, the dynamics of irrigation and precipitation water recovery are described as percentages of the amount of recovered water at the time points T0, T6, and T14, respectively. At T0, 2 hours after the simulated heavy rainfall event, 54.2 % of the recovered irrigation water was found in the top 10 cm. 19.9 % of the recovered water was found at a depth of 10–30 cm. A substantial fraction (25.9 %) however, was already present in the subsoil (30–50 cm depth). Also, at T6 and T14, more than 50 % of the recovered irrigation water was found in the upper 10 cm. At 10–30 cm depth, the percentage of recovered water increased to 31.6 % and 32.6 % at T6 and T14, respectively. However, the absolute amount of Irr_{tot} at 10–30 cm depth

https://doi.org/10.5194/egusphere-2025-2577
Preprint. Discussion started: 3 July 2025

decreased compared to T0. At T6 and T14, only small fractions of the recovered water (4.7 % and 14.4 %, respectively) were found at 30–50 cm depth.

While the irrigation water from the heavy rainfall event (HRE) at T0, Irr_{HRE}, carried a ^{2}H-label, the irrigation water from the following moderate daily rainfall events was unlabeled. Thus, the recovery of the HRE water could be assessed via an isotope mass balance at T0, T8 and T14 from the soil water content, the fraction of the recovered ^{2}H-label, and the amount of simulated heavy rainfall event irrigation water, Irr_{HRE}, (24.3 mm). The recovery was calculated for 10 cm layers of the 50 cm soil cores. The isotope mass balance is presented as the percentage of the simulated heavy rainfall event (24.3 mm) recovered in the soil on days 0, 8, and 14 (T0, T8, T14) on W plots (Figure 3b). The Irr_{HRE} was 108 % at T0, 82 % at T8 and 63 % at T14. In the following, the development of the recovery is described as the percentages of the amount of recovered irrigation water from the heavy rainfall event. At T0, the biggest fraction of HRE irrigation water (30 %) was found in the upper 10 cm of the soil. The rest of the irrigation water was fairly evenly distributed throughout the soil profile: each of the 10 cm depth intervals from 10 to 50 cm containing 15–22 % of the recovered irrigation water. On T8 and 14 only 13 % and 4 % of the recovered Irr_{HRE} were found in the top 10 cm, respectively. Also, in the deeper segments the recovery decreased during the experiment but less pronounced compared to the top 10 cm.

The in situ redox potentials were measured at different depths from 5 cm below ground to 60 cm below ground (Figure 4). In the beginning of the measurements (T0), the in situ redox conditions were oxidizing (> 400 mV vs. SHE) at all depths. In situ redox potentials responded to the irrigation at all measurement points on W plots. In the topsoil layers (0–20 cm below ground) redox potentials mostly declined to reducing conditions within 24 h after the simulated heavy rainfall. In the subsoil (30–50 cm below ground), redox potentials declined more slowly, in most cases within three days.
At 10, 20 and 30 cm soil depth, after the first decline, we observed high temporal and spatial (among sensors) variations in the redox potentials, ranging between oxidizing and moderately reducing conditions, whereas at a depth of 40 to 60 cm below ground, the decline of in situ redox potentials after the irrigation was more constant.
Especially in sensor 1 (plot W1, Figure 4a) at a depth of 10 cm, the daily irrigation and drying of the soil led to strong diurnal changes of the redox potentials between oxidizing and moderately reducing conditions (+200 mV to -100 mV). Between days 10 and 14, the daily irrigation of 5.2 mm was interrupted, and redox potentials rose well into weakly reducing or oxidizing conditions even at soil depths of 30 to 50 cm. At the dry plot (plot D2, Figure 4c and f), the redox potentials remained oxidizing throughout the experiment, except of 10 and 20 cm soil depth at day 10 to 14, when a natural heavy rainfall event hit the experimental plots and removed the protecting foil from plot D2 (but not the other dry treatment plots).

https://doi.org/10.5194/egusphere-2025-2577
Preprint. Discussion started: 3 July 2025

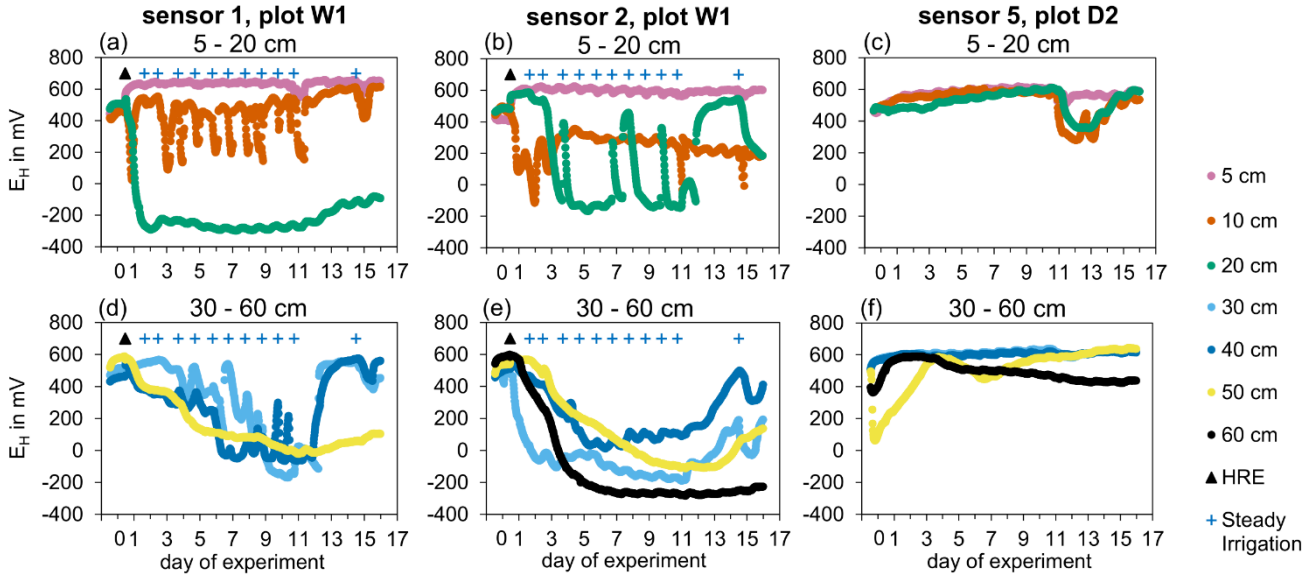

Figure 4: In situ redox potentials (reported as E_H at pH7 in mV vs. SHE) were measured on plot W1 (irrigated with water, sensor 1 and 2) and on plot D2 (dry control, sensor 5) in depths of 5, 10, 20 cm (panels (a) to (c)) and 30, 40, 50, and 60 cm (panels (d) to (f)). The measurements started at experiment day T -1 and are presented until T16. For plot W1, the time points of the simulated heavy rainfall event (HRE, black triangle) and the steady light irrigation (blue crosses) are depicted (panels (a), (b), (d) and (e)).

3.2 Nitrogen Cycle

Ammonium and nitrate mass balances were calculated to evaluate the nitrogen solute transport and the turnover of the two inorganic nitrogen species. Dry control plots on day 0 (DT0) represent the initial state of the soil inorganic nitrogen before irrigation. A comparison of DT0 with irrigated plots on day 0 (WT0), 2 h after the irrigation, therefore, indicates the impact of irrigation on the inorganic nitrogen species distribution across the soil profile.

Two hours after the simulated heavy rainfall, ammonium (Figure 5a) had doubled in the top horizon (0–5 cm), from 0.08 ± 0.03 mg N (DT0) to 0.15 ± 0.02 mg N (WT0) ($p < 0.05$). On W plots at 0–5 cm depth, the ammonium contents further increased to 0.20 ± 0.01 mg N at T6 ($p = 0.058$) and 0.3 ± 0.2 mg N at T14 ($p > 0.05$). Below 5 cm soil depth, only minor changes in soil ammonium content occurred during the experiment, the sum of ammonium over the entire 50 cm soil profile therefore being very similar at DT0, WT0, WT8 and WT14 (0.8–0.9 mg N). However, the sum of ammonium in DT14 (1.2 ± 0.3 mg N) was nearly twice as high as in DT0 ($p > 0.05$). From DT0 to DT14, ammonium mass increased at all depths, three-fold at 0–5 cm ($p < 0.05$) and 1.1-fold to 2.2-fold at greater depth (all $p > 0.05$).

https://doi.org/10.5194/egusphere-2025-2577
Preprint. Discussion started: 3 July 2025

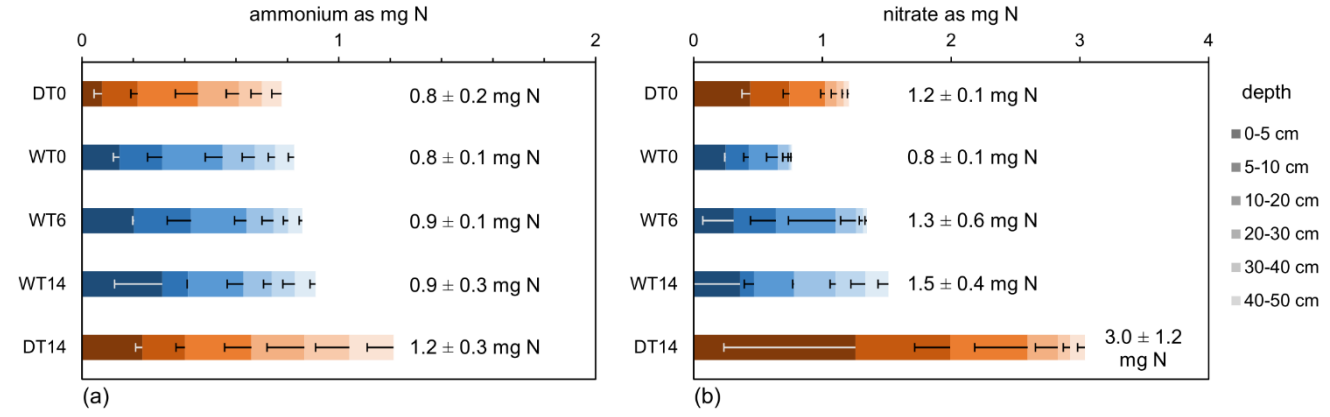

Figure 5: Mass balance of ammonium (panel (a)) and nitrate (panel (b)) (each as mg N per core segment) in cores from dry plots on day 0 and day 14 (orange bars, DT0 and DT14) and on irrigated plots on days 0, 6 and 14 (blue bars, WT0, WT6, WT14). Color shading from dark to light symbolizes increasing depth of the core segments. Displayed are the means of three experimental triplicates and their standard deviations. The sums of ammonium and nitrate contents together with their standard errors in each 50 cm core are displayed on the right of the bars.

Nitrate mass in the whole profile (Figure 5b) decreased by one third shortly after irrigation (1.2 ± 0.1 mg N in DT0 vs. 0.8 ± 0.1 mg N in WT0, $p < 0.05$). This was mostly caused by a 40 % decrease at 0–5 cm and 5–10 cm soil depth (both $p < 0.05$) and an 18 % decrease at 10–20 cm depth ($p > 0.05$). From WT0 to WT14, during ongoing moderate daily irrigation (5.2 mm day^{-1}), the whole-profile nitrate mass almost doubled from 0.8 ± 0.1 mg N to 1.5 ± 0.4 mg N ($p < 0.05$). From WT0 to WT6 nitrate increased at 0–5 cm, 5–10 cm and 10–20 cm while there were no relevant changes below 20 cm depth. From WT6 to WT14, nitrate increased at 0–5 cm and below 20 cm and decreased at 5–10 cm and 10–20 cm (all $p > 0.05$).

On D plots, the sum of nitrate mass showed a 2.5-fold increase from T0 (1.2 ± 0.1 mg N) to T14 (3.0 ± 1.2 mg N) ($p > 0.05$) (Figure 5b). This strong increase of nitrate was mainly due to a strong increase in the upper soil layers: a nearly 3-fold increase in the top segment (0–5 cm) ($p > 0.05$) and a 2.4- and 2.2-fold increase at 5–10 cm ($p < 0.1$) and 10–20 cm ($p > 0.05$), respectively.

3.3 Microbial community composition and extracellular enzyme activities

To assess the effect of a heavy rainfall after a summer drought and the following changes in soil redox potentials on soil microbial community composition and activities, the depth- and time-resolved in situ redox potentials (E_H) were recorded as well as total (on DNA level) and active (on RNA level) soil microbial community composition at depths of 0–10 cm, 20–30 cm and 40–50 cm from dry (D) and wet (W) plots on days 0, 8 and 14.

The 16S rRNA amplicon sequencing resulted in a mean number of 5752 reads per sample for DNA and 6 970 reads per sample for RNA. Due to the large range of reads per sample (DNA: min: 942; max: 12580, and RNA: min: 8; max: 18 224), we

https://doi.org/10.5194/egusphere-2025-2577
Preprint. Discussion started: 3 July 2025

selected only samples with at least 300 reads, thereby reducing the RNA dataset from 54 to 46 samples. These samples contained on average 1 334 different Amplicon Sequence Variants (ASVs) (richness) (Figure 6).

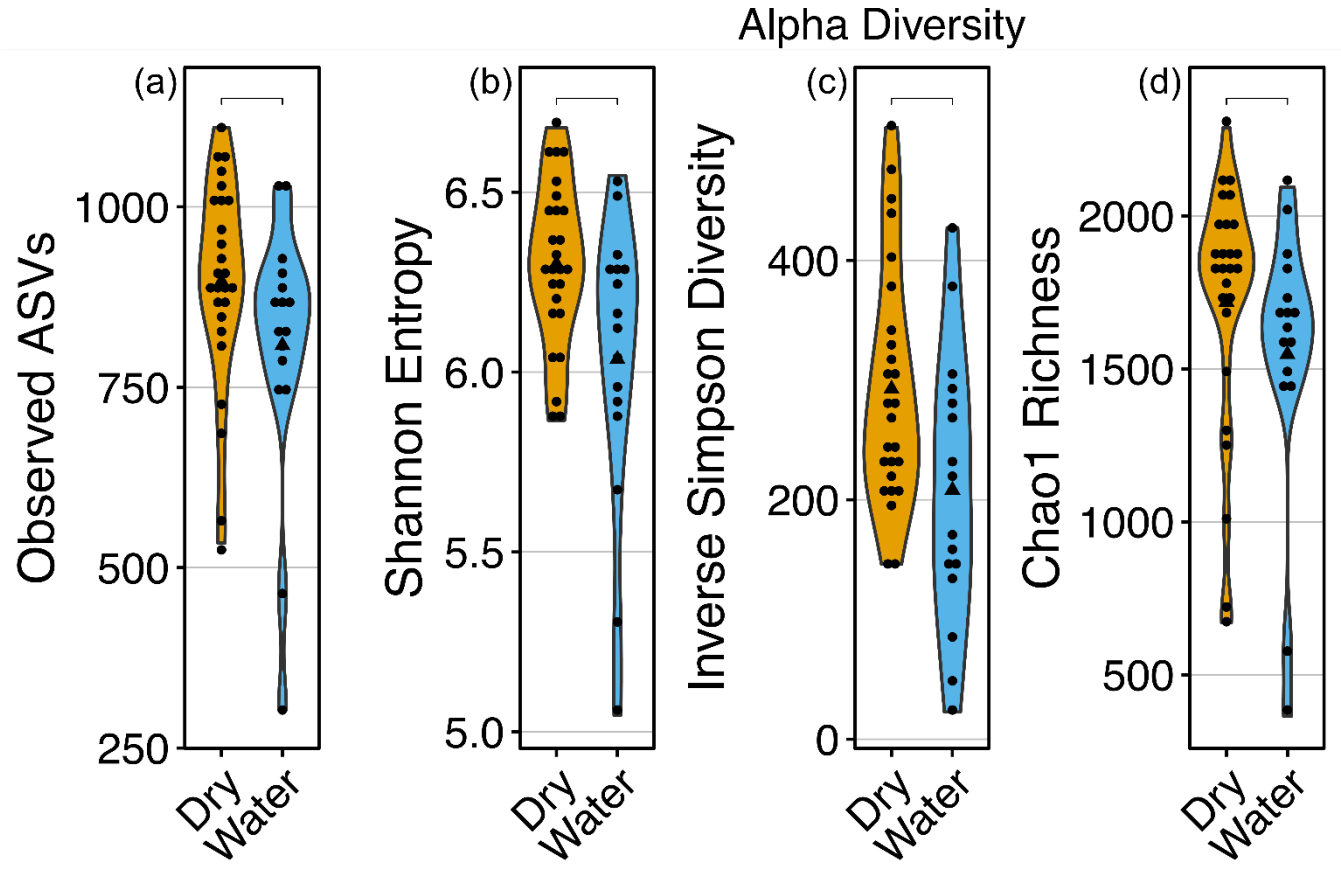

Figure 6: Observed amplicon sequence variants (ASVs) (panel (a)) and different alpha diversity indices (panels (b), (c) and (d)) of microbial communities (RNA) on dry (orange) and watered (blue) plots. Differences between the treatments were not significant ($p > 0.05$) (brackets without asterisk above violins).

Microbial community composition of the different experimental treatments revealed high heterogeneity between sample plots. The soils were dominated by the phyla *Proteobacteria* (mean: 17.4 % SD: 4.7), *Acidobacteriota* (mean: 14.5 % SD: 4.9), *Actinobacteriota* (mean: 13.5 % SD: 7.4) and *Verrucomicrobiota* (mean: 11.5 % SD: 5.2). These were the most abundant phyla independent of wetting, soil depth, and the day of the experiment (Appendix F). At a finer taxonomic resolution, *Pedosphaeraceae* (*Verrucomicrobiota*), unclassified *Vicinamibacterales* (*Acidobacteriota*), *Xiphinematobacteraceae* (*Verrucomicrobiota*) and *Nitrosomonadaceae* (*Gammaproteobacteria*) were the top four bacterial families found throughout all samples with the mean relative abundances varying between 4.6 and 3.2 %.

https://doi.org/10.5194/egusphere-2025-2577
Preprint. Discussion started: 3 July 2025

The common alpha diversity parameters (RNA-fraction) showed only minor differences between dry and wetted soils. Dry soils revealed a little higher diversity compared to the water treated soils (Figure 6). The Shannon diversity of the active (RNA-fraction) prokaryotic communities in dry and wet soils was not significantly different ($p = 0.956$). The DNA and RNA based community data suggest that microbial communities did not change with depth and treatment in terms of composition and active fractions within the short time frame of this study (14-days, Figure 7).

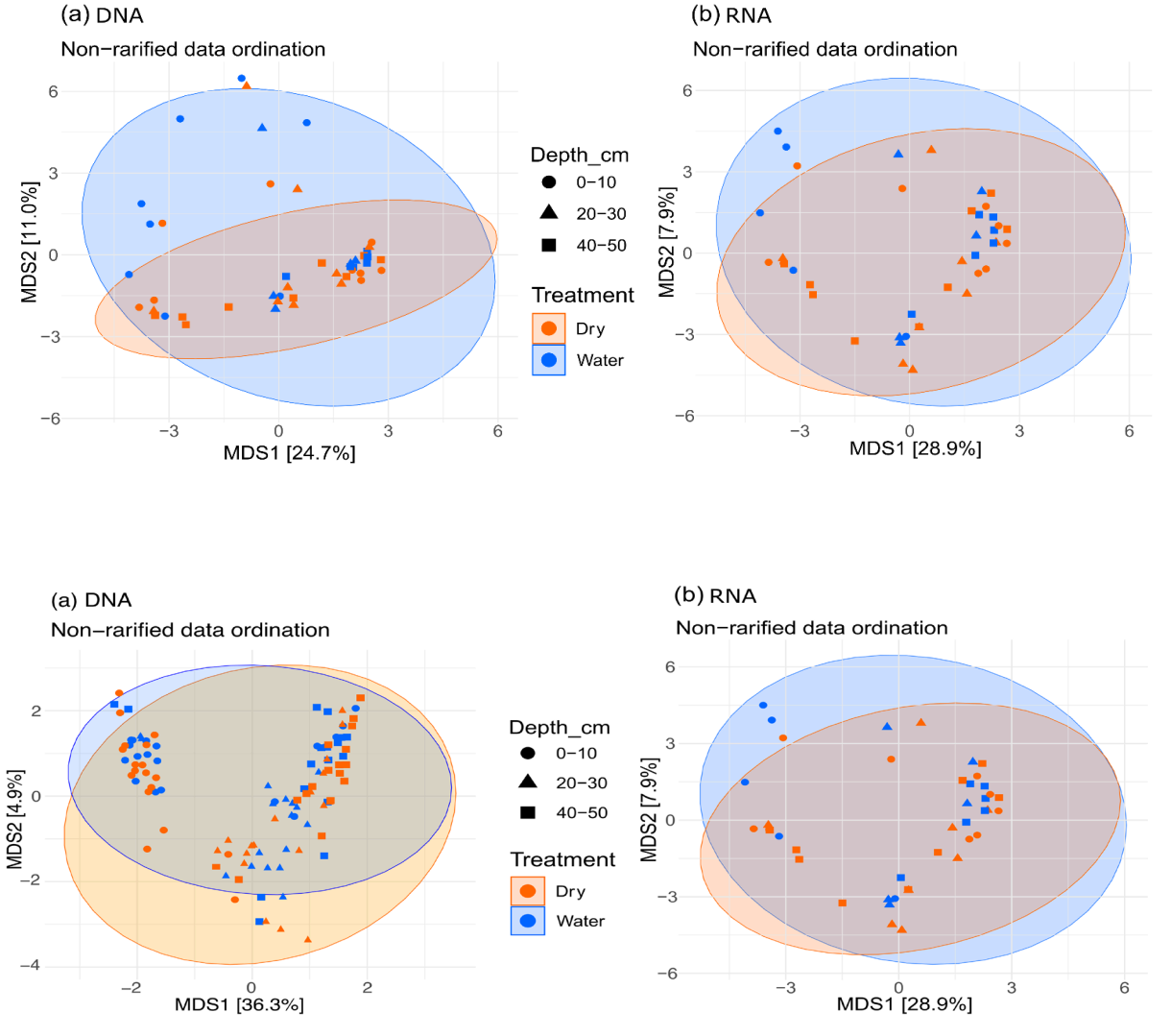

Figure 7: Non-metric multidimensional scaling plots of the microbial community composition (a) on the DNA-level and (b) on the RNA-level at three soil depths (0–10 cm: dots, 20–30 cm: triangles, 40–50 cm: squares) on dry (orange) and irrigated (blue) plots.

https://doi.org/10.5194/egusphere-2025-2577
Preprint. Discussion started: 3 July 2025

The activities of the extracellular enzymes β-glucosidase, exochitinase and acid phosphatase decreased with depth ($p < 0.05$) (Figure 8). β-glucosidase and exochitinase showed significantly higher activities on wet plots than on dry plots ($p < 0.05$), whereas the activity of acid phosphatase did not respond to the irrigation treatment ($p > 0.05$). Time period after rewetting by heavy rainfall was not a significant factor for all three enzymes ($p < 0.05$), indicating that irrigation effects occurred very rapidly and did not recover to pre-treatment levels thereafter. The significant interaction of treatment and soil depth ($p < 0.05$, two-way ANOVA) for β-glucosidase and exochitinase reflects that the wetting treatment effect (stimulation) was strongest in topsoils (0–5 cm) and declined with depth.

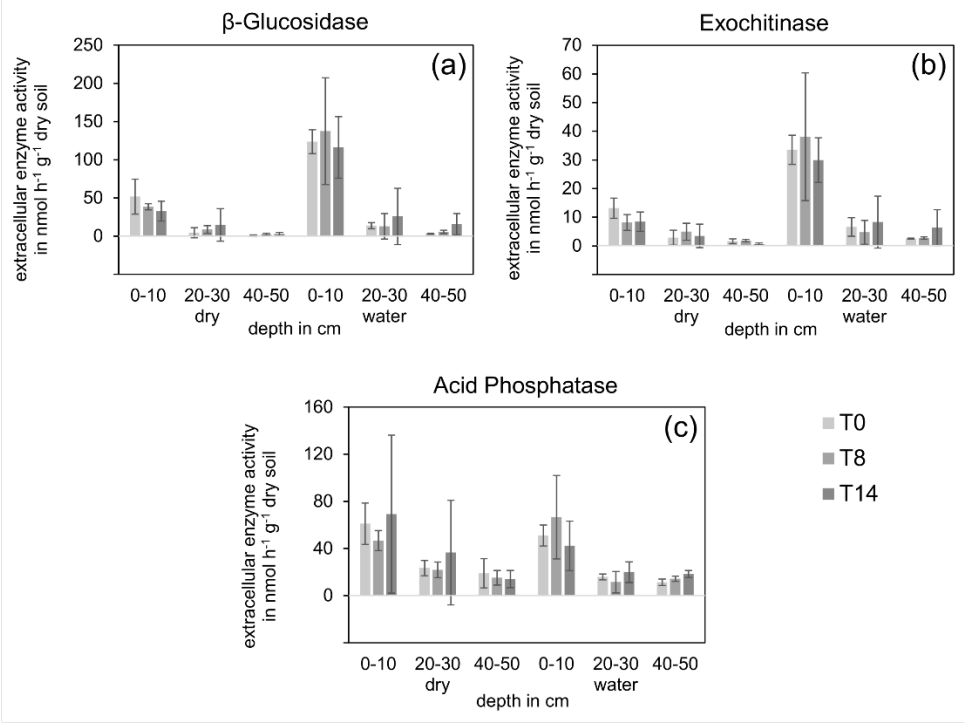

Figure 8: Extracellular enzyme activities of β-glucosidase (panel (a)), exochitinase (panel (b)) and acid phosphatase (panel (c)) at three soil depths on dry and watered plots. The measurement time points day 0, 8 and 14 (T0, T8, T14) are indicated by grey shading from light to dark. Error bars indicate standard deviations of three replicate plots.

https://doi.org/10.5194/egusphere-2025-2577
Preprint. Discussion started: 3 July 2025

4 Discussion

4.1 Water flow and solute transport

Both the water and the isotope mass balance showed that at T0 almost all of the irrigation water was recovered within the profile (Figure 3a and b). It is remarkable that shortly (2 h) after the simulated heavy rainfall, only about half of the irrigation water resided in the topsoil (0–20 cm) while the rest already had reached the subsoil (below 20 cm depth) (Figure 3a). This rapid deep infiltration was facilitated by the pronounced network of shrinkage cracks, which formed in the fine-textured soil due to the preceding drought (Schlögl et al., 2022).

The water mass balance (Figure 3a), following the recovery of the sum of irrigation water and precipitation throughout the whole experimental period (Irr_{tot}), showed that Irr_{tot} decreased from 96 % at T0 to 50 and 32 % at T8 and T14, respectively (Figure 3a). This strong loss of irrigation water can be rationalized by high evaporation rates (ETo = 4.2 mm day^{-1}, see Appendix E) during the course of the experiment. While during the simulated heavy rainfall at T0 (24.3 mm), parts of the irrigation water penetrated down to 50 cm soil depth or even deeper through shrinkage cracks, the continued daily irrigation scheme (5.2 mm day^{-1}) did not penetrate into the subsoil to a larger extent as the shrinkage cracks and thus the preferential flow paths disappeared after initial wetting as shown in Schlögl et al. (2022). Water of subsequent moderate daily irrigations was trapped near the soil surface and thus subject to high evaporation rates (4.2 mm day^{-1}). The pronounced impact of evaporation is supported by the isotope mass balance (Figure 3b), which shows the recovery of the ^{2}H-labeled irrigation water from the simulated heavy rainfall event at T0, Irr_{HRE}. Over the entire 50 cm soil profile, the isotope mass balance indicates slightly lower losses than shown by the water mass balance but also indicates the most pronounced losses in the top 10 cm of the soil (56 % and 86 % at T8 and T14 compared to T0, respectively). Thus, the irrigation rate of 5.2 mm day^{-1} was not high enough to balance the losses by evapotranspiration and seepage during the experimental period as indicated by the decreasing values of the water mass balance with time.

The vertical distribution of ammonium (Figure 5a) and nitrate (Figure 5b) on irrigated and dry plots was affected very differently by solute transport during the simulated heavy rainfall event. Nitrate as a weakly sorbing anion in soils is expected to travel in seepage water without noticeable retardation (Blume et al., 2016). Moreover, rapid transport of dissolved nitrate along preferential flow paths has been shown in earlier studies (Bronswijk et al., 1995; Kelly and Pomes, 1998) and could be the cause of initially decreasing nitrate contents in the topsoil in our experiment (loss of 0.37 mg nitrate-N in the top 20 cm) as evident by the comparison of nitrate in the soil profiles at DT0 (initial state) to WT0 (2 h after the heavy rainfall event) (Figure 5b). However, even though D_2O-labeled water from the simulated heavy rainfall event was found in the subsoil two hours after the event and accompanying hydrological export of nitrate from the topsoil is very likely, we did not observe an accumulation of nitrate in the subsoil. Denitrification is probably not the reason for the disappearance of nitrate at WT0, since the redox potentials in the subsoil were still around 560 ± 30 mV two hours after the heavy rainfall simulation (Blume et al., 2016). Given that crops had been harvested before the start of the experiment and residual roots therefore were inactive, plant

https://doi.org/10.5194/egusphere-2025-2577
Preprint. Discussion started: 3 July 2025

root uptake of nitrate (Cui and Caldwell, 1997) was likely not the cause for the profile-level decrease in nitrate mass. The gradual microbial immobilization of nitrate following severe drought within 2 hours of rewetting may have contributed, but cannot account for such large nitrate "losses". Moreover, this would occur at a time when the Birch effect indicates a flush of microbial metabolites and enzymes into the soil environment, i.e., loss of carbon and nitrogen mass from the microbial community rather than uptake and immobilization (nitrate). Therefore, the unaccounted nitrate was most likely transported below the zone investigated in this study (> 50 cm soil depth) via preferential flow. Directly beneath the upper 2 m clay layer, which comprises the investigated part of the soil profile, a shallow tufaceaous aquifer is located (Martin et al., 2020). The tufaceous aquifer is subject to moderately to strongly reducing conditions (Martin et al., 2020), so denitrification would occur, which could result in the formation of N_2O, a greenhouse gas, or the loss of inorganic nitrogen from the soil in the form of N_2 gas. Constant nitrate input in the groundwater would ultimately lead to a consumption of the reduction capacity of the tufa aquifer and thus to increasing nitrate concentrations in the aquifer. Therefore, nitrate leaching along preferential flow pathways during rewetting after drying can substantially threaten groundwater quality (Sánchez Pérez et al., 2003).

Ammonium (Figure 5a) is subject to cation exchange at negatively charged mineral surfaces including clay minerals. Ammonium therefore is less prone to (downward) transport in soils compared to nitrate (Blume et al., 2016). This retardation prevented the rapid loss of ammonium from the topsoil due to percolation of the irrigation water. The low mobility of ammonium in the soil profile was confirmed when comparing the ammonium mass profiles at DT0 (initial state) to WT0 (2 h after the heavy rain event, Figure 5a) with very similar total ammonium contents and depth distributions in both.

4.2 Nitrogen turnover processes

Soil nitrate and ammonium contents showed a high variability between the three replicate experimental plots; thus, the trends observed in space and time were often not statistically significant (Figure 5). This reflects the high spatial heterogeneity of the distribution of inorganic nitrogen compounds in soils that was also observed by Hergert et al. (1995). At our field site, the heterogeneous distribution (quantified in terms of coefficients of variation) of the simulated heavy rainfall event water was governed by the presence of shrinkage cracks (Schlögl et al., 2022). In the beginning of the experiment, pronounced cracks (up to 1 cm width) were visible at the soil surface and the coefficients of variation of deuterium enrichment of soil water were high. These cracks closed in later states of the experiment while the coefficients of variation of isotope signatures decreased. The coefficients of variation of nitrate and ammonium, however, showed different patterns (Appendix G). For nitrate, the coefficients of variation on the W plots in the top 10 cm were much lower on day 0 than on day 6 and day 14 (Appendix G), reflecting the opposite trend in variance as for the deuterium-enrichment of soil water. For ammonium, no clear trends of the coefficients of variation existed in space and time. The spatial and temporal heterogeneity of the distribution of ammonium and nitrate was therefore not governed by the presence of shrinkage cracks.

The irrigation of dry soil stimulated the mineralization of organic nitrogen (N_{org}) which is reflected by the doubling of ammonium concentration in the topsoil (0–5 cm depth) from DT0 to WT0 (Figure 5a). This increase is in line with the observations made by H. Birch, who described intense nitrogen release upon rewetting of dry soils (Birch, 1958, 1960). The

https://doi.org/10.5194/egusphere-2025-2577
Preprint. Discussion started: 3 July 2025

Birch effect is induced by the mineralization of dead microbial biomass and of osmoregulatory substances that are released by microorganisms upon rewetting (Fierer and Schimel, 2002; Jarvis et al., 2007; Saetre and Stark, 2005; Unger et al., 2010). This is supported by the significant and immediate increase of two extracellular enzymes (β-glucosidase and exochitinase) in soils of W plots compared to D plots within two hours of heavy rainfall simulation (Figure 8), which indicates the release of intracellular compounds (including enzymes) by lysis of a fraction of the microbial cells due to irrigation (Khan et al., 2019). The prolonged increase of ammonium in the topsoil at T6 and T14 (0.05 mg ammonium-N and 0.10 mg ammonium-N, respectively) can be explained by continued net mineralization of organic matter in cropland soils (Booth et al., 2005), by bulk atmospheric deposition of ammonium (average of 0.011 mg ammonium-N per week on the cross sectional area of a sample core (Beyn et al., 2014), for calculation see Appendix H) and by further nitrogen release due to daily drying and rewetting (Birch, 1958; Fierer and Schimel, 2002). Nitrogen fixation as a potential ammonium source was likely negligible, as no legumes were grown at this field site prior to the experiment. At a soil depth of 10 cm and below, ammonium contents, however, did not respond much to irrigation. The reasons can be that (i) there is less labile organic matter at soil depths below 10 cm (Appendix B) and thus less ammonium can be released from mineralization of organic compounds or (ii) that most ammonium present is strongly sorbed to clay minerals and thus is not accessible for nitrification or other microbial-driven processes (Buss et al., 2004; Cavalli et al., 2015). Ammonium can either be bound as exchangeable cation on clay minerals (Blume et al., 2016; Buss et al., 2004) or it can enter the 2:1 clay mineral interlayer (Buss et al., 2004), rendering interlayer ammonium largely recalcitrant to microbial utilization. The high clay and silt content of the studied soils (Appendix C) highlights the high cation-exchange capacity triggered by high surface area and high negative charge density of the clays for ammonium sorption. Alternatively, (iii) ammonium contents can remain relatively constant if the ammonium that is produced per time step is consumed by microbial uptake or oxidized to nitrate under oxic conditions during the same period.

On the W plots, the increase of nitrate mass in the topsoil (0–5 cm) from T0 to T6 and to T14 (by 0.061 mg nitrate-N and 0.05 mg nitrate-N, respectively) (Figure 5b) cannot fully be explained by bulk atmospheric nitrate deposition (0.007 mg nitrate-N per week on the cross sectional area of a sample core (Beyn et al., 2014) for calculation see Appendix I). The increase of nitrate mass at 0–20 cm soil depth at T6 and below 20 cm depth at T14 (Figure 5b) can thus be explained by nitrification (oxidation) of ammonium under oxic conditions (Figure 4) (Cui and Caldwell, 1997). The redox potentials in W plots showed great variations at 10 and 20 cm depth (Figure 4a and b), which occurred between sensors (spatial variations) and between times in single sensors (temporal variations) (Figure 4b). The spatial variations can be explained by oxic and anoxic microsites in otherwise anoxic and oxic environments, respectively (Dorau et al., 2023; Kuzyakov and Blagodatskaya, 2015). Moderate daily fluctuations (e.g., at all sensors at 5 cm), were potentially induced by temperature changes (Dorau et al., 2021). The stronger temporal variations (e.g., sensor 1 at 10 cm (Figure 4a)) followed the daily irrigation and were thus most likely the result of rapid changes between air- and water-filled pore space. Following these changes in oxygen availability, the nitrification rates likely fluctuated. For most of the experimental time, the redox conditions remained above +100 mV, a threshold above which nitrification is active (Hansen et al., 1981), and during these periods we observed an increase in nitrate mass at 5–10 cm and 10–20 cm soil depth at T6. Below 20 cm depth at T6, nitrification did not substantially occur because

https://doi.org/10.5194/egusphere-2025-2577
Preprint. Discussion started: 3 July 2025

redox potentials (Figure 4) were below +100 mV, disfavouring the process. At T14, however, due to the pause in daily light irrigation from the T10 to T14, redox potentials below 20 cm depth rose above the threshold for nitrification related to increasing nitrate contents at T14. Nitrate and ammonium mass changes were therefore partially coupled and nitrate accumulation under oxic conditions was related to ammonium draw down and/or continued mineralization of N_{org} across the whole soil profile.

In summary, the observed nitrogen turnover processes were initially governed by the rewetting of the dry soil and the so-called "Birch effect", which is known to be a short-term effect (Birch, 1958; Cui and Caldwell, 1997; Unger et al., 2010). After approximately one week of the experiment, the nitrogen turnover processes switched from the pulse-driven regime after rewetting to the "usual" redox-driven nitrogen cycling regime governed by oxygen availability as reflected by the drop of in situ redox potentials at greater depth.

The 1.5-fold and 2.5-fold increase of ammonium and nitrate, respectively, on D plots between T0 and T14 is remarkable. The D plots were covered with greenhouse foil between T10 and T14 to prevent wetting by a natural heavy rainfall on the evening of T10 and the following three days. Temperatures below the plastic foil may have increased, activatingmicrobial turnover processes,although we did not observe a shift in microbial community composition in the D plots on T14. Prolonging the experimental drought period prior to irrigation of the dry plots by another two weeks, such as happened on the D plots, might have critically amplified the drying effects on microbial functioning, and therefore have induced a stronger cellular water deficit and soil microbial turnover and death, with concomitant releases of organic and inorganic nitrogen (Figure 5). Alternatively, constant evaporation on the D plots during the experimental period might have induced the rise of soil water transporting dissolved species such as nitrate upwards. On the W plots, this effect was interrupted by the recurring irrigation.

4.3 Microbial communities and activities

Environmental conditions such as temperature, pH, oxygen availability and moisture directly influence soil microbes and thereby affect biogeochemical processes such as nitrogen turnover. The use of stable isotope labelled substrates has shown that soil microbial communities consist of a dynamic fraction that can be activated by rewetting (Aanderud et al., 2015). Revealing these processes and changes in community structure remains challenging. Nucleic acids can persist in the soil environment for long time spans (Carini et al., 2016) hampering diversity estimations. This "inactive" DNA in environmental samples has been linked to either dormant cells (Aanderud et al., 2015) resembling a seed bank or to extracellular nucleic acids that may play a role in other processes (Lennon et al., 2018). In this study, the more short-lived RNA has been used as a proxy of the "active" microbial community fraction. However, we did not find any significant differences between sampling treatments, depth or the length of the experiment (Figure 7). Populations of soil bacteria vary over space, time and in response to environmental changes. Their spatial variation can occur at the micro-scale (Vos et al., 2013), in relation to soil microstructure and organic matter distribution and thus it can be difficult to depict differences between samples. The increase

https://doi.org/10.5194/egusphere-2025-2577
Preprint. Discussion started: 3 July 2025

in activities of the extracellular enzymes β-glucosidase and exochitinase (Figure 8) and of ammonium (Figure 5) on W plots nevertheless indicated an activation of microbial cells by the rewetting.

In dry soils, microbial communities display reduced metabolic activity due to a combination of desiccation stress and reduced substrate diffusion (Schimel et al., 2007). Our data indicate a higher microbial diversity in the dry soils (RNA) than in the irrigated plots (Figure 6), although the differences in diversity were not significant. While rainfall and rewetting of soils have been shown to increase microbial metabolism (Blazewicz et al., 2014; Fierer and Schimel, 2002) they can also exert stress to the microbial communities (Barnard et al., 2013; Schimel, 2018), resulting in the elimination of microbial taxa not adapted to dry-wet cycles (Armstrong et al., 2016; Fierer et al., 2003; Veach and Zeglin, 2020). The microbial communities in our tested soils were not particularly pre-adapted to drought and rewetting – so such a functional selection process within the different taxa present during soil rewetting seems implausible. The reasons for this selection process – from microbial death to soil chemistry as a driver – are still under debate (Schimel, 2018). In our experiment, the induced osmotic stress most likely drove the microbial community shift.

5 Conclusions

Due to climate change, the frequency of droughts and heavy precipitation events is increasing in temperate climates. In our study, we investigated the effects of a heavy rainfall event after a summer drought in a loamy floodplain soil on (i) water flow and solute transport of inorganic nitrogen species, (ii) the occurrence of the Birch effect and the transition towards redox-driven nitrogen turnover processes, and (iii) soil microbial community structure.

Our study showed, that (a) during the heavy rainfall event, water including dissolved nitrate infiltrated into the subsoil along preferential flow paths. This carries the risk of nitrate leaching into the underlying aquifer. (b) Upon rewetting, an increase in inorganic nitrogen (ammonium) occurred as described by the Birch effect. The study confirms that this effect is a short-term effec, lasting a few days at the most until the normal redox-driven nitrogen cycling becomes dominant again. (c) Soil microbial community composition did not respond much to irrigation at both DNA and RNA levels. However, lower diversity indices on irrigated vs. dry plots indicate that stress induced by rewetting lead to some shift in the microbial community towards better adapted taxa. The leaching of nitrate into shallow aquifers upon heavy rainfall events and the shift of the microbial community in cropland soils of Central Europe should be investigated in more detail in follow-up studies.

https://doi.org/10.5194/egusphere-2025-2577
Preprint. Discussion started: 3 July 2025

Appendices

Appendix A: Soil profile in a soil core from the Ammer valley

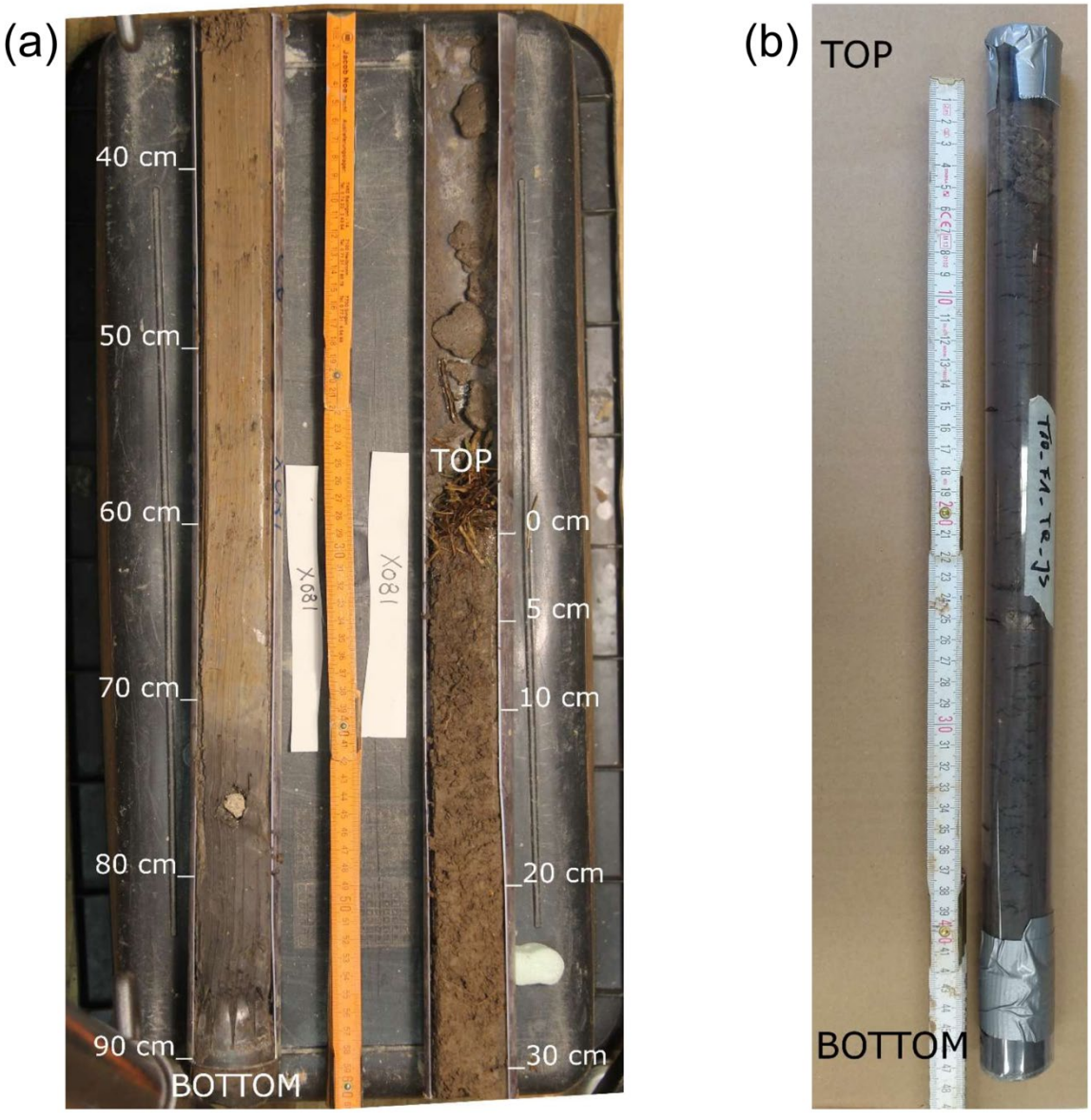

Figure A1: (a) Photo of the upper 90 cm soil profile from a location 100 m NW' of the study site. A 1.20 m deep core was retrieved with a direct push probe (6610 DT, Geoprobe, Salina, Kansas, US), the core was cut in two parts lengthwise for better visibility of the sediments and crosswise at 0.6 m for taking the photo. The missing 30 cm are due to core loss at the bottom of the core. Depth in cm below ground level is depicted besides the core. The upper 70 cm of the core are of uniform red-brown color until at 71 cm the color abruptly changes to grey marking the transition from the Go to the Gr horizon in this Gleysol. Maximum sampling depth of the presented study was 50 cm, which was well within the Go horizon. (The photo is courtesy of S. Klingler and S. Martin.) (b) Photo of a 50 cm soil core from the presented study (plot D1). The uniform red-brown color is visible through the plastic liner. (Figure reproduced from Schlögl et al. (2022) with permission from the Royal Society of Chemistry.)

https://doi.org/10.5194/egusphere-2025-2577
Preprint. Discussion started: 3 July 2025

Appendix B: Soil organic matter

Determination of total organic carbon (TOC)

For the analysis of soil organic matter as total organic carbon (TOC), cores from plots D1–3 and from W1–3 were cut into the following segments: 0–5 cm depth, 5–15 cm, 15–25 cm, 25–35 cm, 35–45 cm, 45–50 cm. The corresponding depth segments from all D plots and from all W plots, respectively, were combined and aliquots of 10 g of soil were freeze-dried (CHRIST ALPHA 1-4, CHRIST, Germany) and were ground to a grain size of < 63 µm with a planetary mill. One 1 g aliquot of each sample was decalcified with 16 % aqueous HCl and subsequently washed with ultrapure water until reaching at minimum a pH of 5. The sample was again dried and then weighed to determine the amount of inorganic carbon. Inorganic carbon was independently determined by acid titration of a second subsample to control the decalcification.

The dried and decalcified subsample was analyzed for TOC in an elemental analyzer (Elementar vario EL, Elementar, Hanau, Germany) with four replicate measurements per sample. TOC was then normalized to the initial dry weight of the sample and expressed as weight%.

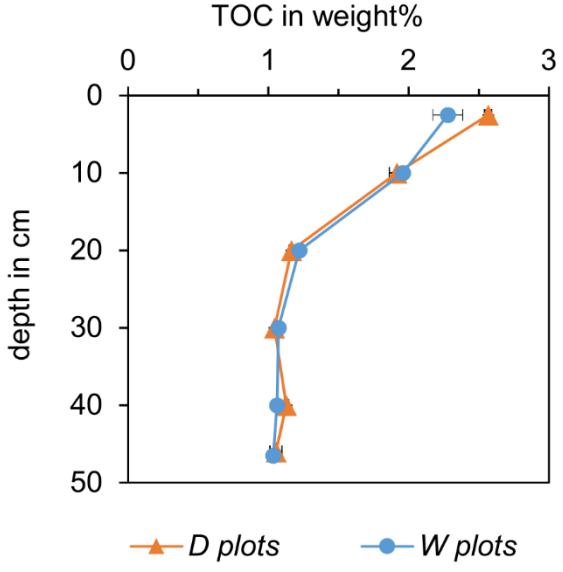

Figure B1: Distribution of soil organic carbon (as TOC) in weight% in a 50 cm depth profile of the studied Gleysol on irrigated plots after 14 days of irrigation (W plots, blue dots) and dry control plots (D plots, orange triangles). (Figure reproduced from Schlögl et al. (2022) with permission from the Royal Society of Chemistry.)

https://doi.org/10.5194/egusphere-2025-2577
Preprint. Discussion started: 3 July 2025

Appendix C: Soil texture

Determination of soil texture

For the analysis of grain size distribution, cores from plots D1–3 and from W1–3 were cut into the following segments: 0–5 cm depth, 5–15 cm, 15–25 cm, 25–35 cm, 35–45 cm, 45–50 cm. The corresponding depth segments from all D plots and from all W plots, respectively, were combined. For each depth segment, grain size analysis was conducted following the German Standard (Din deutsches institut für normung e. v., 2017). Aliquots of 50 g per sample were sieved wet through sieves of 2 mm, 1 mm and 125 µm mesh size to separate the fraction smaller than 125 µm. The fraction bigger than 125 µm was dried and sieved dry through sieves of 500 µm, 250 µm, and 125 µm. The fraction smaller than 125 µm was further analyzed by sedimentation analysis using the integral suspension pressure method (ISP) (Durner et al., 2017) using a PARIO device (Meter Group, Munich, Germany).

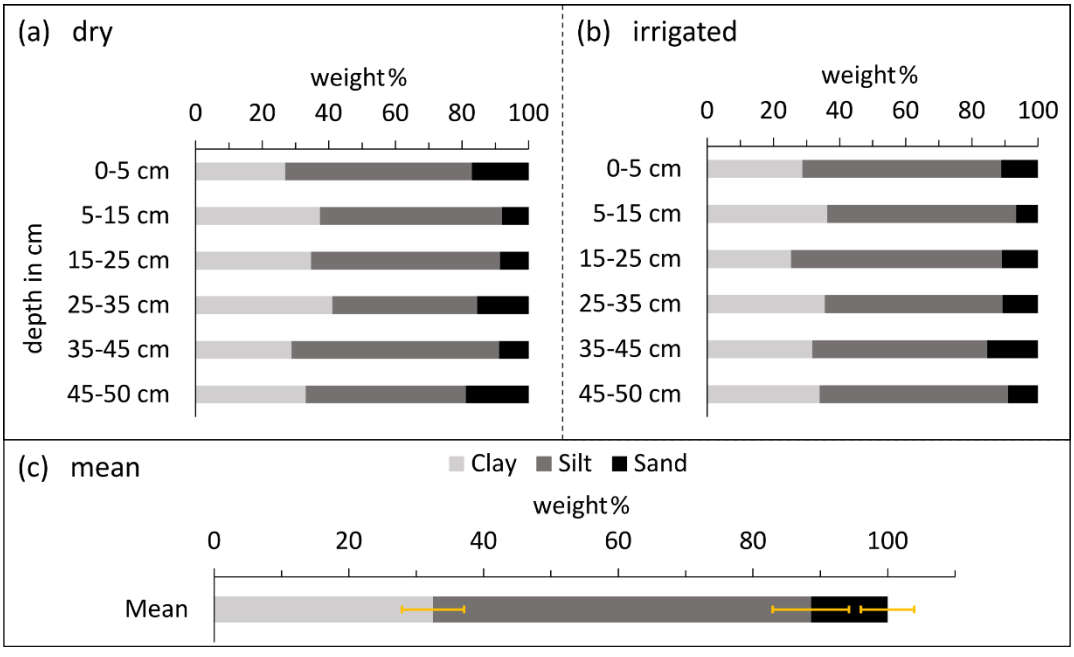

Figure C1: Grain size distribution in weight% of clay (light grey), silt (dark grey), and sand (black). (a) and (b). Grain size distribution in 50 cm soil profiles of the studied Gleysol on dry control plots (a) and irrigated plots (b). (c). Mean values and standard deviations (yellow bars) of the grain size distribution calculated from all samples and depths from dry and irrigated plots (n = 12). The soil is a silty clay loam. (Figure reproduced from Schlögl et al. (2022) with permission from the Royal Society of Chemistry.)

https://doi.org/10.5194/egusphere-2025-2577
Preprint. Discussion started: 3 July 2025

Appendix D: Weather data

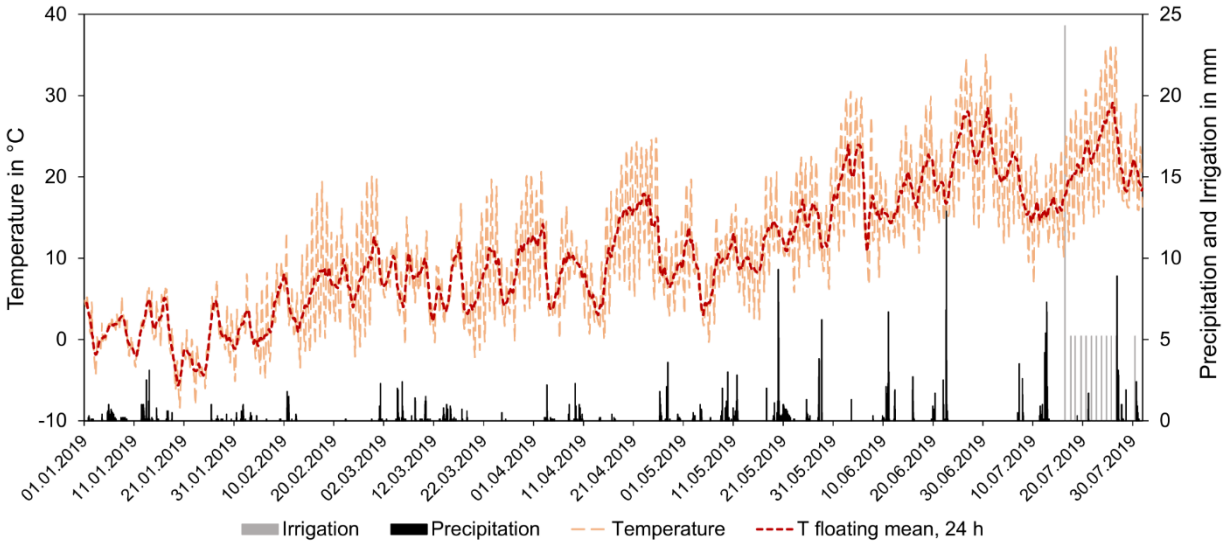

Figure D1: Hourly data of temperature (T) in °C (light red line), natural precipitation (black bars) and irrigation (grey bars) in mm and a 24 h floating mean of the temperature in °C for the period from 1 January 2019 until 31 July 2019 from the weather station in Tübingen-Unterjesingen. The experiment took place from 16 July 2019 until 30 July 2019. (Figure reproduced from Schlögl et al. (2022) with permission from the Royal Society of Chemistry)

Appendix E: Calculation of reference evapotranspiration ETo

The reference evaporation ETo was calculated according to FAO Irrigation and Drainage Paper No. 56 (Allen et al., 1998).

Table E1: Data on temperature (T), relative humidity (RH) and global radiation (Rs) from the weather station in Tübingen-Unterjesingen used for the calculation of the reference evapotranspiration ETo for the period 1 to 31 July 2019

Parameter	Measured value
T_{max} in °C	36.3
T_{mean} in °C	20.4
T_{min} in °C	6.9
RH_{max} in %	100.0
RH_{mean} in %	68.7
RH_{min} in %	26.0

https://doi.org/10.5194/egusphere-2025-2577
Preprint. Discussion started: 3 July 2025

Rs in W m^{-2}	236.0
ETo in mm day^{-1}	4.2

673

674

https://doi.org/10.5194/egusphere-2025-2577
Preprint. Discussion started: 3 July 2025

Appendix F: Microbial community analysis

Relative sequence abundance

The methodology is described in the main text.

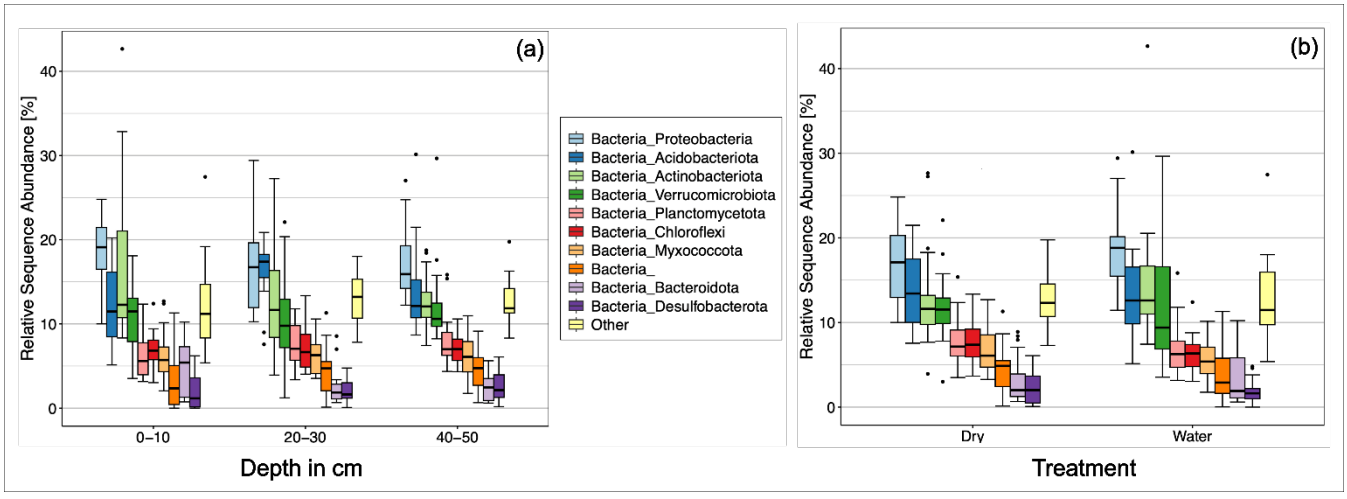

Figure F1: Relative sequence abundance of bacteria phyla in the studied soil sorted by depth (a) and treatment (b).

https://doi.org/10.5194/egusphere-2025-2577
Preprint. Discussion started: 3 July 2025

681

682 **Appendix G: Coefficients of variation of nitrate and ammonium contents on W plots**

683 Coefficients of variation were calculated from mean values and standard deviations (n = 3) of nitrate and ammonium contents
684 along the soil profile.

685

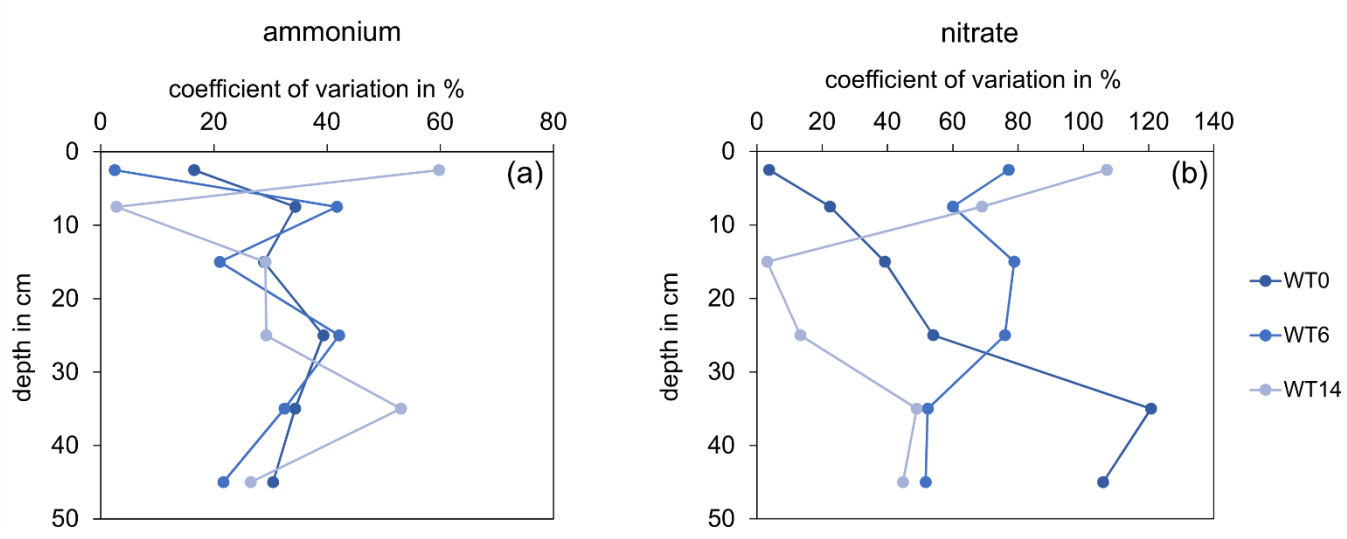

686

687 **Figure G1: Coefficients of variation of ammonium (a) and nitrate (b) contents on W plots at Days T0, T6 and T14.**

688

689

https://doi.org/10.5194/egusphere-2025-2577
Preprint. Discussion started: 3 July 2025

Appendix H: Calculation atmospheric ammonium-N deposition

The atmospheric ammonium-N deposition on the cross-sectional area of an experimental soil core was calculated to evaluate potential sources of ammonium increase observed in the topsoil. Weekly atmospheric ammonium fluxes averaged over one year were taken from Beyn et al. (2014).

Table H1: Calculation of the atmospheric ammonium-N deposition on the cross-sectional area of a soil core with a diameter of 3.5 cm within one week.

Atmospheric ammonium-flux average over one year in µM ammonium m^{-2} per week	Source: Beyn et al. 2014
wet deposition	752
dry deposition	66.7
total	818.7
Molar mass	
M(ammonium) in g mol^{-1}	18.0386
M(N) in g mol^{-1}	14.007
cross sectional area sample core in m^2	0.000962
total ammonium-flux average over one year	
in µg ammonium m^{-2} per week	14768.20
in mg ammonium m^{-2} per week	14.77
in µg ammonium-N m^{-2} per week	11467.53
in mg ammonium-N m^{-2} per week	11.47
on cross-sectional area of a sample core	
in mg ammonium-N per week	0.01103

https://doi.org/10.5194/egusphere-2025-2577
Preprint. Discussion started: 3 July 2025

Appendix I: Calculation atmospheric nitrate-N deposition

The atmospheric nitrate-N deposition on the cross-sectional area of an experimental soil core was calculated to evaluate potential sources of nitrate increase observed in the topsoil. Weekly atmospheric nitrate fluxes averaged over one year were taken from Beyn et al. (2014).

Table I1: Calculation of the atmospheric nitrate-N deposition on the cross-sectional area of a soil core with a diameter of 3.5 cm within one week.

Atmospheric nitrate-flux average over one year in µM nitrate m^{-2} per week	Source: Beyn et al. 2014
wet deposition	468.9
dry deposition	60.6
total	529.5
Molar mass	
M(nitrate) in g mol^{-1}	61.977
M(N) in g mol^{-1}	14.007
cross sectional area sample core in m^2 (radius = 3.5 cm)	0.000962
total nitrate-flux average over one year	
in µg nitrate m^{-2} per week	32816.82
in mg nitrate m^{-2} per week	32.82
in µg nitrate-N m^{-2} per week	7416.71
in mg nitrate-N m^{-2} per week	7.42
on the cross-sectional area of a sample core	
in mg nitrate-N per week	0.0071

https://doi.org/10.5194/egusphere-2025-2577
Preprint. Discussion started: 3 July 2025

Data availability

The data presented in this paper are published in the database of the project "CAMPOS – Catchments as Reactors" at the University of Tübingen, available online (LINK).
Gene amplicon sequencing data, generated by the JMF under Project IDs JMF-2006-4 and JMF-2010-08, were deposited under the BioProject accession number PRJEB87326.

Sample availability?

Supplement link

Author contributions

JS: Conceptualization, Methodology, Investigation, Data curation, Formal analysis, Validation, Visualization, Writing – original draft preparation; CK: For the data on microbial community composition: Data curation, Formal analysis, Visualization, Writing – original draft preparation; LC: Conceptualization, Methodology, Investigation (data on microbial community composition), Data curation (data on microbial community composition); WW: Investigation (extracellular enzyme activities), Formal analysis (extracellular enzyme activities), Writing – review and editing; JP: Sample analysis (extracellular enzyme activities), Writing – review and editing; TB: Sample analysis (extracellular enzyme activities), Writing – review and editing; AK: Funding acquisition, Writing – review and editing; SBH: Conceptualization, Methodology, Funding acquisition, Project administration, Resources, Writing – review and editing; CG: Conceptualization, Methodology, Funding acquisition, Project administration, Resources, Writing – review and editing.

Competing interests

The authors declare that they have no conflict of interest.

Acknowledgements

Financial support was provided by the German Research Foundation by the Collaborative Research Center 1253 CAMPOS Grant Agreement SFB 1253/1 2017 (Project 4: Floodplain Biogeochemistry and Project 6: Controls for the Fate of Agrochemicals in Soils).
We acknowledge the help of M. Jantz during the preparation of the field experiment, of M. Jantz, T. Siller, F. Straub and D. Sanchez Anaya for assistance during the field work, of M. Engelhardt for analyses of soil texture and total organic carbon and for assistance with the extraction of inorganic nitrogen species, and of H. Schulz for freeze drying of soil samples (all from

https://doi.org/10.5194/egusphere-2025-2577
Preprint. Discussion started: 3 July 2025

University of Tübingen). We thank C. Stumpp (University of Natural Resources and Life Sciences, Vienna) for the analysis of soil water stable isotopes and the assistance with the data evaluation, S. Klingler and S. Martin (both University of Tübingen) for providing information on and a photo of one of their cores taken in the Ammer valley, and the landowner for permission to conduct the field work on his farmland.

References

Aanderud, Z. T., Jones, S. E., Fierer, N., and Lennon, J. T.: Resuscitation of the rare biosphere contributes to pulses of ecosystem activity, Frontiers in Microbiology, 6, 10.3389/fmicb.2015.00024, 2015.

Agrarmeteorologie Baden-Württemberg: Wetterdaten, Station Unterjesingen: https://www.wetter-bw.de/Internet/AM/NotesBwAM.nsf/bwweb/4262596897754529c1257ca8002f9d19?OpenDocument, last access: 14.10.2021.

Allen, R. G., Pereira, L. S., Raes, D., and Smith, M.: FAO Irrigation and drainage paper 56 - Crop evapotranspiration - Guidelines for computing crop water requirements, FAO - Food and Agriculture Organization of the United Nations, Rome1998.

American Meteorological Society: "Rain". Glossary of Meteorology: https://glossary.ametsoc.org/wiki/Rain, last access: 03.02.2024.

Armstrong, A., Valverde, A., Ramond, J.-B., Makhalanyane, T. P., Jansson, J. K., Hopkins, D. W., Aspray, T. J., Seely, M., Trindade, M. I., and Cowan, D. A.: Temporal dynamics of hot desert microbial communities reveal structural and functional responses to water input, Scientific Reports, 6, 34434, 10.1038/srep34434, 2016.

Baldwin, D. S. and Mitchell, A. M.: The effects of drying and re-flooding on the sediment and soil nutrient dynamics of lowland river–floodplain systems: a synthesis, Regulated Rivers: Research & Management, 16, 457-467, https://doi.org/10.1002/1099-1646(200009/10)16:5<457::AID-RRR597>3.0.CO;2-B, 2000.

Barnard, R. L., Osborne, C. A., and Firestone, M. K.: Responses of soil bacterial and fungal communities to extreme desiccation and rewetting, The ISME Journal, 7, 2229-2241, 10.1038/ismej.2013.104, 2013.

Beven, K. and Germann, P.: Macropores and water flow in soils revisited, Water Resources Research, 49, 3071-3092, https://doi.org/10.1002/wrcr.20156, 2013.

Beyn, F., Matthias, V., and Dähnke, K.: Changes in atmospheric nitrate deposition in Germany – An isotopic perspective, Environmental Pollution, 194, 1-10, https://doi.org/10.1016/j.envpol.2014.06.043, 2014.

Birch, H. F.: The effect of soil drying on humus decomposition and nitrogen availability, Plant and Soil, 10, 9-31, 10.1007/BF01343734, 1958.

Birch, H. F.: Nitrification in soils after different periods of dryness, Plant and Soil, 12, 81-96, 10.1007/BF01377763, 1960.

Blazewicz, S. J., Schwartz, E., and Firestone, M. K.: Growth and death of bacteria and fungi underlie rainfall-induced carbon dioxide pulses from seasonally dried soil, Ecology, 95, 1162-1172, https://doi.org/10.1890/13-1031.1, 2014.

Blume, H.-P., Brümmer, G. W., Fleige, H., Horn, R., Kandeler, E., Kögel-Knabner, I., Kretzschmar, R., Stahr, K., and Wilke, B.-M.: Scheffer/Schachtschabel Soil Science, Springer, Berlin, Heidelberg, Berlin, Heidelberg, XVIII, 618 pp., https://doi.org/10.1007/978-3-642-30942-7, 2016.

Booth, M. S., Stark, J. M., and Rastetter, E.: CONTROLS ON NITROGEN CYCLING IN TERRESTRIAL ECOSYSTEMS: A SYNTHETIC ANALYSIS OF LITERATURE DATA, Ecological Monographs, 75, 139-157, https://doi.org/10.1890/04-0988, 2005.

Bronswijk, J. J. B., Hamminga, W., and Oostindie, K.: Rapid nutrient leaching to groundwater and surface water in clay soil areas, European Journal of Agronomy, 4, 431-439, https://doi.org/10.1016/S1161-0301(14)80095-6, 1995.

Buss, S., Herbert, A., Morgan, P., Thornton, S., and Smith, J.: A Review of Ammonium Attenuation in Soil and Groundwater, Quarterly Journal of Engineering Geology and Hydrogeology - Q J ENG GEOL HYDROGEOL, 37, 347-359, 10.1144/1470-9236/04-005, 2004.

https://doi.org/10.5194/egusphere-2025-2577
Preprint. Discussion started: 3 July 2025

781 Callahan, B. J., McMurdie, P. J., and Holmes, S. P.: Exact sequence variants should replace operational taxonomic units in
782 marker-gene data analysis, The ISME Journal, 11, 2639-2643, 10.1038/ismej.2017.119, 2017.
783 Carini, P., Marsden, P. J., Leff, J. W., Morgan, E. E., Strickland, M. S., and Fierer, N.: Relic DNA is abundant in soil and
784 obscures estimates of soil microbial diversity, Nature Microbiology, 2, 16242, 10.1038/nmicrobiol.2016.242, 2016.
785 Cavalli, D., Consolati, G., Marino, P., and Bechini, L.: Measurement and simulation of soluble, exchangeable, and non-
786 exchangeable ammonium in three soils, Geoderma, 259-260, 116-125, https://doi.org/10.1016/j.geoderma.2015.05.011, 2015.
787 Coby, A. J., Picardal, F., Shelobolina, E., Xu, H., and Roden, E. E.: Repeated anaerobic microbial redox cycling of iron, Appl
788 Environ Microbiol, 77, 6036-6042, 10.1128/AEM.00276-11, 2011.
789 Coumou, D. and Rahmstorf, S.: A decade of weather extremes, Nature Climate Change, 2, 491-496, 10.1038/nclimate1452,
790 2012.
791 Cui, M. and Caldwell, M. M.: A large ephemeral release of nitrogen upon wetting of dry soil and corresponding root responses
792 in the field, Plant and Soil, 191, 291-299, 10.1023/A:1004290705961, 1997.
793 DIN Deutsches Institut für Normung e. V.: DIN EN ISO 17892-4 Geotechnical investigation and testing - Laboratory testing
794 of soil - Part 4: Determination of particle size distribution, Beuth, Berlin, 7, 2017.
795 Dorau, K., Bohn, B., Weihermüller, L., and Mansfeldt, T.: Temperature-induced diurnal redox potential in soil, Environmental
796 Science: Processes & Impacts, 23, 1782-1790, 10.1039/D1EM00254F, 2021.
797 Dorau, K., Uteau, D., Maisch, M., Kappler, A., Peth, S., and Mansfeldt, T.: Redoxtrons – An experimental system to study
798 redox processes within the capillary fringe, European Journal of Soil Science, 74, e13347, https://doi.org/10.1111/ejss.13347,
799 2023.
800 Durner, W., Iden, S. C., and von Unold, G.: The integral suspension pressure method (ISP) for precise particle-size analysis
801 by gravitational sedimentation, Water Resources Research, 53, 33-48, https://doi.org/10.1002/2016WR019830, 2017.
802 Fierer, N. and Schimel, J. P.: Effects of drying–rewetting frequency on soil carbon and nitrogen transformations, Soil Biology
803 and Biochemistry, 34, 777-787, https://doi.org/10.1016/S0038-0717(02)00007-X, 2002.
804 Fierer, N., Schimel, J. P., and Holden, P. A.: Influence of Drying–Rewetting Frequency on Soil Bacterial Community
805 Structure, Microbial Ecology, 45, 63-71, 10.1007/s00248-002-1007-2, 2003.
806 German Meteorological Service (DWD): Monatliche Mittel/Summen, Niederschlag, Station Stuttgart-Echterdingen:
807 https://www.dwd.de/DE/leistungen/kvo/baden_wuerttemberg.html?nn=480164, last access: 02.02.2024.
808 Geyer, O. F., Gwinner, M. P., Geyer, M., and Ellwanger, D.: Geologie von Baden-Württemberg, 5., völlig neu bearb. Aufl. /
809 hrsg. von Matthias Geyer ... unter Mitarb. von Dietrich Ellwanger ... Schweizerbart, Stuttgart, 627 pp.2011.
810 Grathwohl, P., Rügner, H., Wöhling, T., Osenbrück, K., Schwientek, M., Gayler, S., Wollschläger, U., Selle, B., Pause, M.,
811 Delfs, J.-O., Grzeschik, M., Weller, U., Ivanov, M., Cirpka, O. A., Maier, U., Kuch, B., Nowak, W., Wulfmeyer, V., Warrach-
812 Sagi, K., Streck, T., Attinger, S., Bilke, L., Dietrich, P., Fleckenstein, J. H., Kalbacher, T., Kolditz, O., Rink, K., Samaniego,
813 L., Vogel, H.-J., Werban, U., and Teutsch, G.: Catchments as reactors: a comprehensive approach for water fluxes and solute
814 turnover, Environmental Earth Sciences, 69, 317-333, 10.1007/s12665-013-2281-7, 2013.
815 Hansen, J. I., Henriksen, K., and Blackburn, T. H.: Seasonal Distribution of Nitrifying Bacteria and Rates of Nitrification in
816 Coastal Marine Sediments, Microbial Ecology, 7, 297-304, 1981.
817 Hefting, M., Clément, J. C., Dowrick, D., Cosandey, A. C., Bernal, S., Cimpian, C., Tatur, A., Burt, T. P., and Pinay, G.: Water
818 table elevation controls on soil nitrogen cycling in riparian wetlands along a European climatic gradient, Biogeochemistry, 67,
819 113-134, 10.1023/B:BIOG.0000015320.69868.33, 2004.
820 Hergert, G. W., Ferguson, R. B., Shapiro, C. A., Penas, E. J., and Anderson, F. B.: Classical Statistical and Geostatistical
821 Analysis of Soil Nitrate-N Spatial Variability, in: Site-Specific Management for Agricultural Systems, ASA, CSSA, and SSSA
822 Books, 175-186, https://doi.org/10.2134/1995.site-specificmanagement.c13, 1995.
823 Horton, R. M., Mankin, J. S., Lesk, C., Coffel, E., and Raymond, C.: A Review of Recent Advances in Research on Extreme
824 Heat Events, Current Climate Change Reports, 2, 242-259, 10.1007/s40641-016-0042-x, 2016.
825 Jarvis, N., Koestel, J., and Larsbo, M.: Understanding Preferential Flow in the Vadose Zone: Recent Advances and Future
826 Prospects, Vadose Zone Journal, 15, vzj2016.2009.0075, https://doi.org/10.2136/vzj2016.09.0075, 2016.
827 Jarvis, P., Rey, A., Petsikos, C., Wingate, L., Rayment, M., Pereira, J., Banza, J., David, J., Miglietta, F., Borghetti, M., Manca,
828 G., and Valentini, R.: Drying and wetting of Mediterranean soils stimulates decomposition and carbon dioxide emission: the
829 "Birch effect"†, Tree Physiology, 27, 929-940, 10.1093/treephys/27.7.929, 2007.

https://doi.org/10.5194/egusphere-2025-2577
Preprint. Discussion started: 3 July 2025

Kelly, B. P. and Pomes, M. L.: Preferential Flow and Transport of Nitrate and Bromide in Clay pan Soil, Groundwater, 36, 484-494, https://doi.org/10.1111/j.1745-6584.1998.tb02820.x, 1998.
Khan, S. U., Hooda, P. S., Blackwell, M. S. A., and Busquets, R.: Microbial Biomass Responses to Soil Drying-Rewetting and Phosphorus Leaching, Frontiers in Environmental Science, 7, 10.3389/fenvs.2019.00133, 2019.
Kuzyakov, Y. and Blagodatskaya, E.: Microbial hotspots and hot moments in soil: Concept & review, Soil Biology and Biochemistry, 83, 184-199, https://doi.org/10.1016/j.soilbio.2015.01.025, 2015.
Lair, G. J., Zehetner, F., Fiebig, M., Gerzabek, M. H., van Gestel, C. A. M., Hein, T., Hohensinner, S., Hsu, P., Jones, K. C., Jordan, G., Koelmans, A. A., Poot, A., Slijkerman, D. M. E., Totsche, K. U., Bondar-Kunze, E., and Barth, J. A. C.: How do long-term development and periodical changes of river–floodplain systems affect the fate of contaminants? Results from European rivers, Environmental Pollution, 157, 3336-3346, https://doi.org/10.1016/j.envpol.2009.06.004, 2009.
Lennon, J. T., Muscarella, M. E., Placella, S. A., and Lehmkuhl, B. K.: How, When, and Where Relic DNA Affects Microbial Diversity, mBio, 9, 10.1128/mbio.00637-00618, 10.1128/mbio.00637-18, 2018.
Mansfeldt, T.: In situ long-term redox potential measurements in a dyked marsh soil, Journal of Plant Nutrition and Soil Science, 166, 210-219, https://doi.org/10.1002/jpln.200390031, 2003.
Martin, S., Klingler, S., Dietrich, P., Leven, C., and Cirpka, O. A.: Structural controls on the hydrogeological functioning of a floodplain, Hydrogeology Journal, 28, 2675-2696, 10.1007/s10040-020-02225-8, 2020.
Moche, M., Gutknecht, J., Schulz, E., Langer, U., and Rinklebe, J.: Monthly dynamics of microbial community structure and their controlling factors in three floodplain soils, Soil Biology and Biochemistry, 90, 169-178, https://doi.org/10.1016/j.soilbio.2015.07.006, 2015.
Nimmo, J. R.: The processes of preferential flow in the unsaturated zone, Soil Science Society of America Journal, 85, 1-27, https://doi.org/10.1002/saj2.20143, 2021.
Perkins, S. E., Alexander, L. V., and Nairn, J. R.: Increasing frequency, intensity and duration of observed global heatwaves and warm spells, Geophysical Research Letters, 39, https://doi.org/10.1029/2012GL053361, 2012.
Pjevac, P., Schauberger, C., Poghosyan, L., Herbold, C. W., van Kessel, M. A. H. J., Daebeler, A., Steinberger, M., Jetten, M. S. M., Lücker, S., Wagner, M., and Daims, H.: AmoA-Targeted Polymerase Chain Reaction Primers for the Specific Detection and Quantification of Comammox Nitrospira in the Environment, Frontiers in Microbiology, 8, 10.3389/fmicb.2017.01508, 2017.
Rinklebe, J., and Langer, U.: Microbial diversity in three floodplain soils at the Elbe River (Germany), Soil Biology and Biochemistry, 38, 2144-2151, https://doi.org/10.1016/j.soilbio.2006.01.018, 2006.
Saetre, P. and Stark, J. M.: Microbial dynamics and carbon and nitrogen cycling following re-wetting of soils beneath two semi-arid plant species, Oecologia, 142, 247-260, 10.1007/s00442-004-1718-9, 2005.
Sánchez Pérez, J. M., Antiguedad, I., Arrate, I., Garcı, x, a-Linares, C., and Morell, I.: The influence of nitrate leaching through unsaturated soil on groundwater pollution in an agricultural area of the Basque country: a case study, Science of The Total Environment, 317, 173-187, https://doi.org/10.1016/S0048-9697(03)00262-6, 2003.
Schimel, J., Balser, T. C., and Wallenstein, M.: MICROBIAL STRESS-RESPONSE PHYSIOLOGY AND ITS IMPLICATIONS FOR ECOSYSTEM FUNCTION, Ecology, 88, 1386-1394, https://doi.org/10.1890/06-0219, 2007.
Schimel, J. P.: Life in Dry Soils: Effects of Drought on Soil Microbial Communities and Processes, Annual Review of Ecology, Evolution, and Systematics, 49, 409-432, 10.1146/annurev-ecolsys-110617-062614, 2018.
Schlögl, J., Wimmer, B., Cramaro, L., Wirsching, J., Poll, C., Pagel, H., Kandeler, E., Huhn, C., Griebler, C., Stumpp, C., and Haderlein, S. B.: Heavy rainfall following a summer drought stimulates soil redox dynamics and facilitates rapid and deep translocation of glyphosate in floodplain soils, Environmental Science: Processes & Impacts, 24, 825-838, 10.1039/D1EM00527H, 2022.
Schwientek, M., Osenbrück, K., and Fleischer, M.: Investigating hydrological drivers of nitrate export dynamics in two agricultural catchments in Germany using high-frequency data series, Environmental Earth Sciences, 69, 381-393, 10.1007/s12665-013-2322-2, 2013.
Tian, Y., Schindlbacher, A., Malo, C. U., Shi, C., Heinzle, J., Kwatcho Kengdo, S., Inselsbacher, E., Borken, W., and Wanek, W.: Long-term warming of a forest soil reduces microbial biomass and its carbon and nitrogen use efficiencies, Soil Biology and Biochemistry, 184, 109109, https://doi.org/10.1016/j.soilbio.2023.109109, 2023.

https://doi.org/10.5194/egusphere-2025-2577
Preprint. Discussion started: 3 July 2025

878 Tournier, E., Amenc, L., Pablo, A. L., Legname, E., Blanchart, E., Plassard, C., Robin, A., and Bernard, L.: Modification of a
879 commercial DNA extraction kit for safe and rapid recovery of DNA and RNA simultaneously from soil, without the use of
880 harmful solvents, MethodsX, 2, 182-191, https://doi.org/10.1016/j.mex.2015.03.007, 2015.
881 Unger, S., Máguas, C., Pereira, J. S., David, T. S., and Werner, C.: The influence of precipitation pulses on soil respiration –
882 Assessing the "Birch effect" by stable carbon isotopes, Soil Biology and Biochemistry, 42, 1800-1810,
883 https://doi.org/10.1016/j.soilbio.2010.06.019, 2010.
884 Veach, A. M. and Zeglin, L. H.: Historical Drought Affects Microbial Population Dynamics and Activity During Soil Drying
885 and Re-Wet, Microbial Ecology, 79, 662-674, 10.1007/s00248-019-01432-5, 2020.
886 Venterink, H. O., Wiegman, F., Van der Lee, G. E. M., and Vermaat, J. E.: Role of Active Floodplains for Nutrient Retention
887 in the River Rhine, Journal of Environmental Quality, 32, 1430-1435, https://doi.org/10.2134/jeq2003.1430, 2003.
888 Vos, M., Wolf, A. B., Jennings, S. J., and Kowalchuk, G. A.: Micro-scale determinants of bacterial diversity in soil, FEMS
889 Microbiology Reviews, 37, 936-954, 10.1111/1574-6976.12023, 2013.
890 Wassenaar, L. I., Hendry, M. J., Chostner, V. L., and Lis, G. P.: High Resolution Pore Water δ2H and δ18O Measurements by
891 H2O(liquid)−H2O(vapor) Equilibration Laser Spectroscopy, Environmental Science & Technology, 42, 9262-9267,
892 10.1021/es802065s, 2008.
893 Wirsching, J., Wimmer, B., Ditterich, F., Schlögl, J., Martin-Laurent, F., Huhn, C., Haderlein, S., Kandeler, E., and Poll, C.:
894 13C assimilation as well as functional gene abundance and expression elucidate the biodegradation of glyphosate in a field
895 experiment, Environmental Pollution, 306, 119382, https://doi.org/10.1016/j.envpol.2022.119382, 2022.